

AD-A047 397

SCIENCE APPLICATIONS INC LA JOLLA CALIF
MULTIMODE MODELING OF THE WATER MOLECULE.(U)
AUG 77 D ROGOVIN, T STEPHENS, W WILSON

F/G 20/10

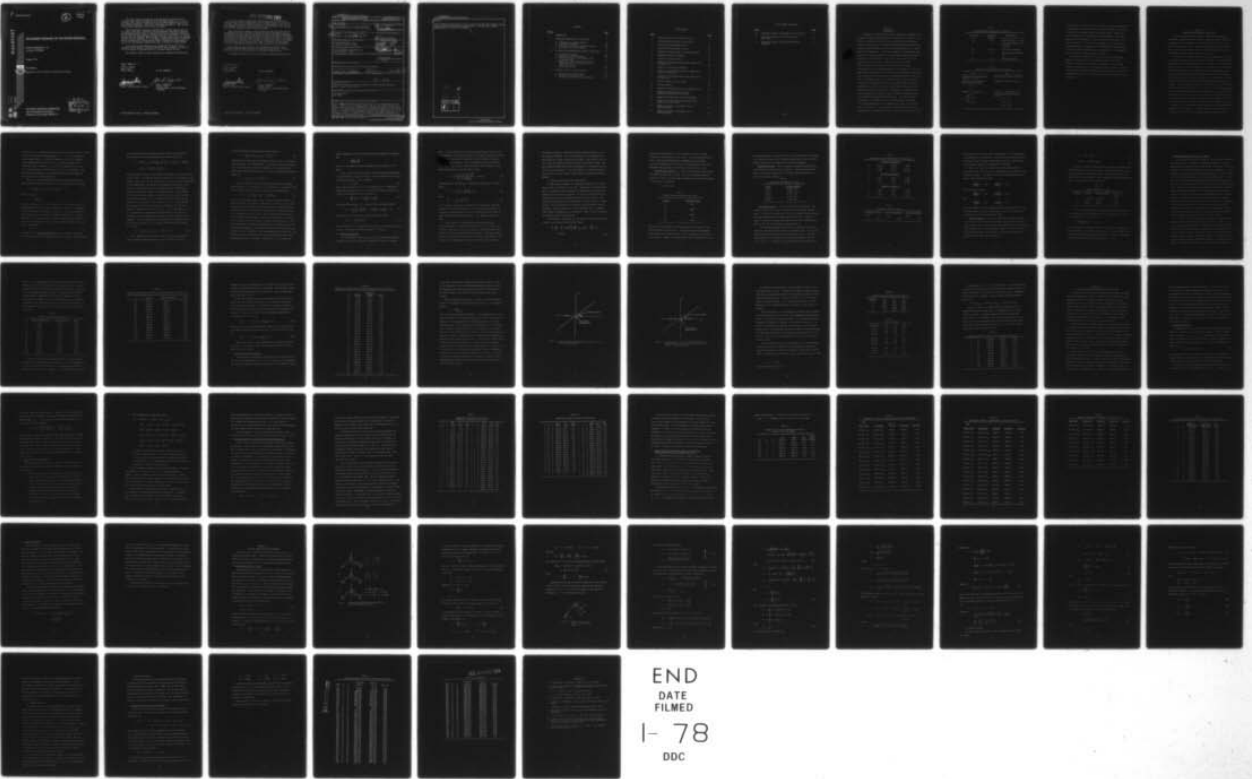
F29601-75-C-0132

UNCLASSIFIED

AFWL-TR-76-253

NL

1 OF 1
AD
A047397



22

AFWL-TR-76-253

2

AD-E 200 051 ✓
AFWL-TR-
76-253

AD A 0 4 7 3 9 7

MULTIMODE MODELING OF THE WATER MOLECULE

Science Applications, Inc.
La Jolla, CA 92038

August 1977

Final Report

Approved for public release; distribution unlimited.



AD NO. _____
DDC FILE COPY

AIR FORCE WEAPONS LABORATORY
Air Force Systems Command
Kirtland Air Force Base, NM 87117


DDC
RECEIVED
DEC 12 1977
B

This final report was prepared by the University of Arizona Optical Sciences Center, Tuscon, Arizona and by Science Applications, Inc., La Jolla, California under Contract F29601-75-C-0132, Job Order 33260915, with the Air Force Weapons Laboratory, Kirtland Air Force Base, New Mexico. Major Gilbert (LRO) was the Laboratory Project Officer-in-Charge.

When US Government drawings, specifications, or other data are used for any purpose other than a definitely related Government procurement operation, the Government thereby incurs no responsibility nor any obligation whatsoever, and the fact that the Government may have formulated, furnished, or in any way supplied the said drawings, specifications, or other data is not to be regarded by implication or otherwise as in any manner licensing the holder or any other person or corporation or conveying any rights or permission to manufacture, use, or sell any patented invention that may in any way be related thereto.

This report has been reviewed by the Information Office (OI) and is releasable to the National Technical Information Service (NTIS). At NTIS, it will be available to the general public, including foreign nations.

This technical report has been reviewed and is approved for publication.

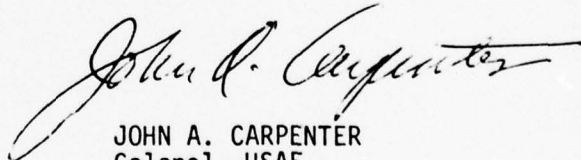


KEITH G. GILBERT
Major, USAF
Project Officer

FOR THE COMMANDER



LAWRENCE SHER
Chief, ALL Beam Control Branch



JOHN A. CARPENTER
Colonel, USAF
Assistant Chief, Laser Development
Division

DO NOT RETURN THIS COPY. RETAIN OR DESTROY.

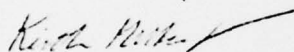
BEST AVAILABLE COPY

This final report was prepared by the University of Arizona Optical Sciences Center, Tuscon, Arizona and by Science Applications, Inc., La Jolla, California under Contract F29601-75-C-0132, Job Order 33260915, with the Air Force Weapons Laboratory, Kirtland Air Force Base, New Mexico. Major Gilbert (LRO) was the Laboratory Project Officer-in-Charge.

When US Government drawings, specifications, or other data are used for any purpose other than a definitely related Government procurement operation, the Government thereby incurs no responsibility nor any obligation whatsoever, and the fact that the Government may have formulated, furnished, or in any way supplied the said drawings, specifications, or other data is not to be regarded by implication or otherwise as in any manner licensing the holder or any other person or corporation or conveying any rights or permission to manufacture, use, or sell any patented invention that may in any way be related thereto.

This report has been reviewed by the Information Office (OI) and is releasable to the National Technical Information Service (NTIS). At NTIS, it will be available to the general public, including foreign nations.

This technical report has been reviewed and is approved for publication.

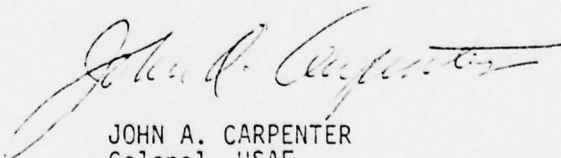


KEITH G. GILBERT
Major, USAF
Project Officer

FOR THE COMMANDER



LAWRENCE SHER
Chief, ALL Beam Control Branch



JOHN A. CARPENTER
Colonel, USAF
Assistant Chief, Laser Development
Division

DO NOT RETURN THIS COPY. RETAIN OR DESTROY.

UNCLASSIFIED

SECURITY CLASSIFICATION OF THIS PAGE (When Data Entered)

REPORT DOCUMENTATION PAGE		READ INSTRUCTIONS BEFORE COMPLETING FORM
1. REPORT NUMBER AFWL-TR-76-253	2. GOVT ACCESSION NO.	3. RECIPIENT'S CATALOG NUMBER
4. TITLE (and Subtitle) MULTIMODE MODELING OF THE WATER MOLECULE.	5. TYPE OF REPORT & PERIOD COVERED Final Report.	6. PERFORMING ORG. REPORT NUMBER
7. AUTHOR(s) D./Rogovin, T./Stephens W. W./Wilson	8. CONTRACT OR GRANT NUMBER(s) F29601-75-C-0132	9. PROGRAM ELEMENT, PROJECT, TASK AREA & WORK UNIT NUMBERS 626012F 33260915
9. PERFORMING ORGANIZATION NAME AND ADDRESS Science Applications, Inc. La Jolla, California 92038	10. REPORT DATE Aug 1977	11. NUMBER OF PAGES 72
11. CONTROLLING OFFICE NAME AND ADDRESS Air Force Weapons Laboratory (LRO) Kirtland AFB, NM 87117	12. SECURITY CLASS. (of this report) Unclassified	13. DECLASSIFICATION DOWNGRADING SCHEDULE
14. MONITORING AGENCY NAME & ADDRESS (if different from Controlling Office)	16. DISTRIBUTION STATEMENT (of this Report) Approved for public release; distribution unlimited.	
15. SECURITY CLASS. (of this report)	17. DISTRIBUTION STATEMENT (of the abstract entered in Block 20, if different from Report) 388 862	
18. SUPPLEMENTARY NOTES The initial contractor was the University of Arizona, Optical Sciences Center, Tucson, Arizona 85721.	19. KEY WORDS (Continue on reverse side if necessary and identify by block number) Multimode modeling Water vapor	
20. ABSTRACT (Continue on reverse side if necessary and identify by block number) In this final report we presents three approaches to multimode modeling water vapor. These are (1) A correlated bend approach that treats fluctuations in the bend angle as well as correlations of the bending mode with the OH stretch mode. Only a single "effective" nuclear coordinate is used. (2) A model that treats all three vibrational degrees of freedom, mode-mode coupling as well as molecular rotation. In addition, the effects of centrifugal distortion are included in a nonperturbative manner. (3) A phenomenological approach based		

CONTENTS

<u>Section</u>		<u>Page</u>
I	INTRODUCTION	1
II	CORRELATED BENDER MODEL OF WATER VAPOR	4
	A. Foundations for Quantum Analysis	6
	B. Vibrational Structure	10
	C. Rotational-Vibrational Structure of Water	18
	D. The Role of the Nuclear Masses	23
III	A PREDICTIVE PHENOMENOLOGICAL MODEL OF WATER VAPOR	31
	A. Theoretical Foundation	32
	B. Comparison to Other Approaches	35
	C. Preliminary Results on the Bending Mode Vibrational Bands	37
	D. Present Data Base, Vibrational Bands of Significance for HF Transitions, and an Iterative Data Link	41
	E. Future Applications	49
IV	MULTIMODE MODEL OF THE WATER MOLECULE	51
	A. Multimode Hamiltonian of Water	51
	B. Description of Computer Code	61
	C. Molecular Potential Surface and Geometry	64

LIST OF TABLES

<u>Table</u>		<u>Page</u>
1	Spectrum of Water Vapor from 2 to 10.6 μm	2
2	Vibrational Characteristics of CO and CO ₂	2
3	Potential Energy Constants Display	13
4	Ground State Even Moments of (q-q ₀)	14
5	Rotational Constant Matrix for Correlated Bender	15
6	Experimental Rotation Constants	15
7	Geometric Structure of Water	17
8	Comparison of Rotational-Vibrational Energy Levels in (000) State	19
9	Effects of Centrifugal Distortion	21
10	Comparison of High-Energy Rotational-Vibrational Levels in (000) State	22
11	Comparison of Rotational-Vibrational Energy Levels in (010) State	24
12	Potential Energy Constants Display	29
13	Rotation Matrices	29
14	Rotational-Vibrational Energy Level Structure in D ₂ O	30
15	Comparison of Observed and Calculated Rotational-Vibrational Energy Levels	39
16	Comparison of High-Lying Levels to Experiment	40
17	Comparison of Low-Lying Rotational-Vibrational Levels in the (110) State	42
18	Comparison of Model to Experiment for CO ₂ Laser Wavelengths	45
19	Comparison of Model to Experiment at CO Laser Wavelengths	44

LIST OF TABLES (Continued)

<u>Table</u>		<u>Page</u>
20	Comparison of Model to Experiment in the DF Region	45
21	Rotational-Vibrational Level Structure for (001) State	46
22	Rotational Energies Calculated from Rotation Constants	66

SECTION I
INTRODUCTION

Propagation of infrared laser radiation through the atmosphere is to a greater or lesser extent hindered by the presence of water vapor. Specifically, molecular absorption on the various rotational-vibrational levels of water give rise to significant atmospheric attenuation of high-intensity laser radiation at CO₂, CO, and HF frequencies and to a lesser extent at DF frequencies. A detailed examination of the molecular structure of water vapor indicates that the following vibrational bands are of importance: the ground state, (010), (100), (001), (020) as well as mixed states (110) and (011). Different regions of the water vapor absorption spectrum involve different vibrational bands. Furthermore, due to the extreme asymmetry of this molecule as well as its large rotation constants, the level structure is sufficiently complex that often transitions from the same band cover different regions of the spectrum. For example, ground to ν_2 transitions arise in both the CO₂ and CO regions of the spectrum, and this in conjunction with the extreme centrifugal distortion that occurs in water demands that one treat the molecular rotations with great care. Furthermore, as noted above, the different regions of the spectrum involve different vibrational bands, and the different vibrational states interact. (See Tables 1 and 2.) Consequently, a multimode model of the water molecule is required for a proper description of those regions of the water vapor spectrum that are of interest. In this report we describe three different approaches used in developing a multimode model of water vapor along with

Table 1
Spectrum of Water Vapor from 2 to 10.6 μm

Frequency	Wavelength (μm)	Description
CO_2	10.6	kinetic cooling, V-V rates of N_2 off H_2O water vapor continuum
CO	4.8-5.0	water vapor continuum
DF	3-4	water vapor continuum and HDO
HF	2-3	water vapor lines

Table 2
Vibrational Characteristics of CO and CO_2

CO	CO_2
Numerous hot band transitions at 5 μm : $\nu_2 \rightarrow 2\nu_2$	Hot band transitions at 9.28 μm :
Many cross-band transitions involving the hot band:	Ground to ν_2 dominates 10.6 μm
$\nu_2 \rightarrow \nu_3$	
$\nu_2 \rightarrow \nu_1$	
Ground to ν_2 transitions	Ground to ν_2 dominates 9.28 μm
$\nu_2 \rightarrow \nu_1$	Pure rotational transitions at 9.28 μm :
$\nu_2 \rightarrow \nu_3$	$11_{-5} \rightarrow 12_3$
$0 \rightarrow \nu_2$	$13_{-11} \rightarrow 14_{-3}$
$\nu_2 \rightarrow 2\nu_2$	$14_{-10} \rightarrow 15_{-8}$

relevant results. The first involves the use of a single coordinate that is so designed to simulate all three vibrational degrees of freedom and is applied to the ground and (010) vibrational states. These states play a significant role for CO₂, CO, and DF frequencies. The second approach involves treating all three vibrational coordinates as well as their interactions. Finally, a third approach that is motivated by a vibrational analysis is presented. This technique is phenomenological in nature and offers excellent hope for a global (1 to 20 μm) model of water vapor that is highly accurate and reliable.

In Section II we present our results for the correlated bender approach to water and discuss the physical content of our model. In Section III we discuss our predictive phenomenology for a multimode treatment of water and display preliminary results. Finally, in Section IV we present a multimode treatment of the water molecule, describe the computer programs, outline the physical content of the model and exhibit its results.

SECTION II
CORRELATED BENDER MODEL OF WATER VAPOR

In this section we present a model for treating the rotational-vibrational structure and spectra that arise from bond angle fluctuations in molecular systems and apply it to the specific case of water. Our model is based on the motion of the bond angle and the correlation of this motion with the stretch modes and involves the description of a single internuclear coordinate (but is multimode in nature).

Specifically, we present a model of the water molecule that is based on the relative motion of the two protons, with respect to each other, and the coupling of this motion to the molecular rotation. In this model, the classical trajectory of the two protons is a straight path. This implies that the OH bond length is no longer fixed at some average value, but is allowed to fluctuate along with the bond angle. Since we are describing this motion by means of a single coordinate, it is clear that such a model contains correlations between the OH bond length and the bond angle fluctuations. The most interesting feature of this model, which we shall refer to as a correlated bender model, is that it yields a more accurate description of the rotational-vibrational level structure of the ground and (010) vibrational states in the sense that its predicted energies and molecular geometry are in better agreement with experiment than previous work. Typical values are within 0.5% for all rotational states through $J = 10$ and 1% through $J = 15$. In constructing this model, the only experimental data used were the first three ($J = 0$) bending mode vibrational energy level spacings as well as the A and B rotation constants associated with the

ground vibrational state. Note that the C rotation constant of the ground state as well as all of the rotation constants of the (010) vibrational state are predicted quantities. It is found that the correlated bender predicts a ground state C-rotation constant that lies within 0.01 cm^{-1} of the measured value. Furthermore, the excited state rotation constants are found to lie within 1% of the experimental values.

In Section IIA we present our model of water vapor and discuss its physical characteristics. Specifically, we begin with the Darling-Dennison rotational-vibrational Hamiltonian for a polyatomic molecule (ref. 1) and in a series of steps reduce it to two different forms that are appropriate for treating our two models of water. Following this we present a detailed description of the vibrational structure of H_2O that our model predicts. Specifically, we present the potential energy surface, the characteristic structure of the proton-proton motion, and the rotation-constant matrices associated with this model.

In Section IIB we consider the rotational level structure within the ground and (010) vibrational bands. Specifically, we obtain the vibrational-rotational energies and wave functions using a modified theory of the asymmetric rotor. In particular, we diagonalize the vibrational-rotational energies together, not individually as is usually done. This combined diagonalization is particularly important for H_2O inasmuch as the rotational-vibrational interaction is extremely strong and consequently plays an important role in the rotational-vibrational level structure. We present tables of predicted versus experimental values of the various rotational states of H_2O . To determine how much of the rotational-vibrational interaction is accounted for in our models, we also include

in these tables the values of the rigid rotor energies. These were obtained by replacing all off-diagonal elements of the rotation matrices with zero (ref. 2). A comparison of the various energies demonstrates that for the 10_10 state, about 90% of the rotational-vibrational interaction is accounted for in the correlated bender model.

In Section IIC we discuss the symmetric isotopes D_2O and T_2O . This enables us to examine certain features of the correlated bender model that are mass dependent, specifically, the degree of centrifugal distortion, the molecular structure, and the correlation between the bond angle fluctuations and the OH stretch motion.

A. Foundations for Quantum Analysis

In this section we present our model of the water molecule that is based on the fluctuations of a single coordinate. For convenience, we have subdivided this section into two parts. In Section IIA-1 we construct the quantum mechanical Hamiltonian that we use to model the rotational-vibrational structure and spectrum of the water molecule. In Section IIB-1 we use the Hamiltonian to derive various properties of H_2O that depend on the intranuclear motion.

1. Rotational-Vibrational Hamiltonian

Our starting point is the Darling-Dennison (ref. 1) rotational-vibrational Hamiltonian for a nonlinear polyatomic molecule

$$\begin{aligned}
 H = & \frac{1}{2} \sum_{\alpha\beta} u^{\frac{1}{4}} (\pi_{\alpha} - \pi_{\alpha}') u_{\alpha\beta} u^{-\frac{1}{2}} (\pi_{\beta} - \pi_{\beta}') u^{\frac{1}{4}} \\
 & + \frac{1}{2} u^{\frac{1}{4}} \sum_k p_k u^{-\frac{1}{2}} p_k u^{\frac{1}{4}} + V
 \end{aligned} \tag{1}$$

In Equation (1), V is the molecular potential energy surface, which is a function of all the normal coordinates $\{Q_k | k = 1, \dots\}$, P_k is the corresponding conjugate momenta, Π_α is the α th component of the total rotational-angular momentum of the molecule, and π_α is the α th component of the vibrational-angular momentum. $\mu_{\alpha\beta}$ is the (α, β) component of the effective reciprocal moment of inertia tensor, and μ is its determinant. These quantities are determined by the molecular configuration and therefore are functions of the normal coordinates.

Watson (ref. 3) has demonstrated that for nonlinear molecules the Darling-Dennison Hamiltonian can be cast in the following very useful form

$$H = \frac{1}{2} \sum_{\alpha\beta} (\Pi_\alpha - \pi_\alpha) \mu_{\alpha\beta} (\Pi_\beta - \pi_\beta) + \frac{1}{2} \sum_k P_k^2 + V + U \quad (2)$$

where U is given by

$$U = -\frac{\hbar}{8} \sum_\alpha \mu_{\alpha\alpha} \quad (3)$$

It follows from Equation (3) that U depends only on the nuclear masses, the molecular geometry, and the normal coordinates. Hence, it is independent of the various momenta that appear in Equation (1), and as noted by Watson, can be regarded as an effective mass-dependent potential that we formally include in V . We note that, when a molecule assumes a linear configuration, the nuclear moment of inertia associated with that direction vanishes and as a consequence,

$$U \rightarrow -\infty \quad (4)$$

The presence of an infinitely attractive term in a molecular Hamiltonian is disturbing and on physical grounds should not be present. The resolution

of this difficulty can be obtained by noting that for linear molecules the rotational-vibrational Hamiltonian can be written as (ref. 4)

$$\begin{aligned}
 H = & \frac{1}{2} \left(\mu \pi_x \pi_x + \frac{1}{2} i \hbar \xi_x \right) (\pi_x - \pi_x) - i \hbar \xi_x + \frac{1}{2} \mu (\pi_y - \pi_y - \frac{1}{2} i \hbar \xi_y) \\
 & \times \left(\pi_y - \pi_y + \frac{1}{2} i \hbar \xi_y \right) + \frac{1}{2} \sum_k p_k^2 + V, \quad (5)
 \end{aligned}$$

where the quantities ξ_x and ξ_y are defined in Reference 4 and do not directly concern us here. The important feature of Equation (5) is the absence of the effective potential U . We note that Equations (2) and (5) differ considerably in form, particularly with regard to the rotational structure [π_z is not present in (5)] and the fact that linear molecules have an additional vibrational degree with respect to nonlinear molecules. These features are well known; our only purpose in discussing them is to point out that the molecular Hamiltonian is well behaved in the sense that it does not contain terms that diverge to minus infinity (ref. 4). In the remainder of this paper we shall group the effective potential U with the actual potential V and refer to the sum, $U + V$, as V . It is this quantity that will be obtained by a least-squares fitting technique. We note, as a consequence, that the potential energy that we eventually obtain is mass dependent. We can investigate this mass dependence by examining the isotopic species D_2O and T_2O . This is done in Section IIC. Thus, Equation (2) now reads

$$H = \frac{1}{2} \sum_{\alpha\beta} (\pi_\alpha - \pi_\alpha) \mu_{\alpha\beta} (\pi_\beta - \pi_\beta) + \frac{1}{2} \sum p_k^2 + V \quad (2a)$$

For a symmetrical molecule such as H_2O , it is easy to demonstrate that the reciprocal moment of inertia tensor is diagonal, thus the

molecular rotational-vibrational Hamiltonian reduces to

$$H = \frac{1}{2} \sum_{\alpha} (\pi_{\alpha} - \pi_{\alpha}') \mu_{\alpha\alpha} (\pi_{\alpha} - \pi_{\alpha}') + \frac{1}{2} \sum_{k} p_k^2 + V \quad (6)$$

Furthermore, we shall neglect both Coriolis forces as well as vibrational-angular momentum. This approximation is justified on the grounds that the bulk of the rotational-vibrational interaction in the (000) and (010) bands arises from centrifugal distortion. Thus, our molecular Hamiltonian reduces to

$$H = \frac{1}{2} \sum_{\alpha} (\pi_{\alpha}^2 / \mu_{\alpha\alpha}) + \frac{1}{2} \sum_{k} p_k^2 + V \quad (7)$$

Next, we consider the kinetic energy associated with the bending mode vibration, i.e., fluctuations in the bond angle θ . We begin by noting that the moment of inertia $I(\theta)$ associated with the bending mode is

$$I(\theta) = \frac{1}{2} m_H r^2 [m_O + m_H(1 + \cos\theta)] / M_{H_2O} \quad (8)$$

where r is the OH bond length, m_H , m_O , and M_{H_2O} the atomic hydrogen, oxygen, and molecular water masses, respectively. We note that $I(\theta)$ depends only weakly on the bond angle θ and in Section IIB, we demonstrate that the contribution to the vibrational energy that arises from fluctuations in $I(\theta)$ amounts to less than 0.08%. Now, the Born-Oppenheimer theorem (ref. 5) states that the coupling between the electron and nuclear motion is on the order of $(m_e/M)^{1/2}$, where M is some suitable nuclear mass. Thus, errors encountered in neglecting fluctuations of $I(\theta)$ appear to be of the same order of magnitude as corrections that arise from deviations from an adiabatic model. Furthermore, as we shall demonstrate in Section IIB, this energy is an order of magnitude smaller than any other that arises from approximations made in this paper. Consequently, we shall ignore the

angular dependence of $I(\theta)$ and use for the kinetic energy of the bending mode

$$T = - \frac{\hbar^2}{2I(\theta_0)} \frac{\partial^2}{\partial \theta^2},$$

where I_0 is the moment of inertia evaluated at a fixed angle θ_0 (see below).

Next, we note that for situations involving large amplitude changes in the bond angle, as occurs in water, it is more convenient to work with a length than an angle. Thus, we define

$$x = 2r \sin\theta/2, \quad (9)$$

which varies from zero to $2r$ as θ varies from zero to π . Defining the dimensionless coordinate q as x/r , we find that the kinetic energy associated with fluctuations of the bond angle is

$$T = \frac{\hbar^2}{2I_0} \left\{ [1 - q^2/4] \frac{d^2}{dq^2} - \frac{1}{4} q \frac{d}{dq} \right\} \quad (10)$$

Fixing the OH bond length at r , we obtain the following Hamiltonian

$$H_1 = \frac{1}{2} \sum_{\alpha} \frac{\hbar^2 \alpha^2}{\mu_{\alpha\alpha}} - \frac{\hbar^2}{2I_0} \left\{ [1 - q^2/4] \frac{d^2}{dq^2} - \frac{1}{4} q \frac{d}{dq} \right\} + V(q) \quad (11)$$

where $V_1(q)$ will be taken to be a power series of the form

$$V_1(q) = \sum_{n=2}^{\infty} a_n [q - q_0]^n \quad (12)$$

Note that Equation (12) corresponds to an expansion in Legendre polynomials, $P_n(\cos\theta)$, which form a complete set where $q_0 = 2\sin\theta_0/2$.

B. Vibrational Structure

In our correlated bender model, we wish to constrain the classical trajectory in such a way that the two protons will travel in straight

paths. Now, the variation of the kinetic energy operator with q as well as the presence of the first derivative term $q(d/dq)$ in Equation (10) reflect that the classical trajectory of the two protons is along the circle of radius r . Thus, if we neglect the first derivative term and fix q to a value q_0 (discussed below), then classically we are describing the motion of two particles of mass μ

$$\mu = m_H \frac{m_O + m_H \left[1 - (q_0/2)^2 \right]}{\left[1 - (q_0/2)^2 \right] M_{H_2O}} \approx 2.398 m_H \quad (13)$$

traveling along a straight path. The molecular Hamiltonian H for this model is

$$H = + \frac{1}{2} \sum_{\alpha} \frac{\pi_{\alpha}^2}{\mu_{\alpha\alpha}} - \frac{\hbar^2}{\mu r^2} \frac{d}{dq^2} + V(q) \quad (14)$$

where

$$V(q) = \sum_{n=2} a_n (q - q_0)^n \quad (15)$$

$q_0 = 2 \sin \theta_0 / 2$, r and a_n are so chosen that the eigenvalues and eigenvectors of H will least-squares fit the A and B rotation constants of the ground vibrational state as well as the spacings between ground and first three excited bending mode states. This completely defines our model.

At first glance, one might suppose that our model as manifested in Equation (14) represents an approximation. This, however, is not the case. Specifically, we are now including correlations between fluctuations of the OH bond length and the bond angle. This follows immediately if one considers the structure of the motion of the protons. Specifically, for configurations in which the protons extend beyond the

equilibrium distance q_0 the OH bond distance increases whereas if $q < q_0$, this distance decreases. Thus, the fluctuations in the bond angle and bond length are strongly correlated in our model. Note, however, that we do not take into account the complete motion of the OH bond length. Thus, this correlated bender model should be regarded as an alternative description of the water molecule. This interpretation is clearly justified by the fact that our model renders a highly accurate description of the H_2O molecule.

1. Vibration Structure of the Water Molecule

In this section we present the vibrational properties of the water molecule that are predicted by our model. Specifically, we display tables of (1) the potential energy constants, (2) expectation values of various moments of the vibrational coordinate, (3) the A, B, and C rotation constant matrices, and (4) the geometric structure of the molecule. For convenience, these properties are displayed in separate sections. Before doing so, we first describe our least-squares (self-consistent) fitting technique. Our basic approach is to first determine the $J = 0$ bending mode vibration eigenfunctions and eigenvalues. This is done by iterating the following steps self-consistently.

The vibrational eigenvalues (E_n) and eigenfunctions $u_n(q)$ are determined by first solving the Schrödinger equation

$$\left\{ -\frac{\hbar^2}{2I_0} \left[1 - (q_0/2)^2 \right] \frac{d^2}{dq^2} + \sum_{n=2} a_n (q - q_0)^n \right\} u_n(q) = E_n u_n(q) \quad (16)$$

Taking these eigenfunctions, we then evaluate the A and B rotation constants in the ground and (0,1,0) states. We then determine the optimum q_0 , mean OH bond length, and a_n by demanding that the eigenvalues and eigenfunctions of (16) and (17) least-squares fit the above-mentioned energy spacings and rotational constants (refs. 1,2,6).

Potential Energy Function. In Table 3 we display the various potential energy constants for our model. Note that the bending mode (described by θ) does not undergo simple harmonic motion since the bond angle θ is related to q by means of

$$\theta = 2 \sin^{-1} (q/2)$$

Table 3
Potential Energy Constants Display [cm^{-1}]

<u>Parameter</u>	<u>Correlated Bender</u>
a_2	45510
a_3	0
a_4	-30833
a_5	0
a_6	-23665
a_7	0
a_8	1820

We note that including terms of the form $a_9(q-q_0)^9$ and $a_{10}(q-q_0)^{10}$ did not significantly improve the fit. At first glance, one might suppose that a power series expansion in $(q-q_0)$ would be sufficient to fit three level spacings. However, our scheme requires that the ground state A and

B rotation constants be accounted for as well, and this affects the fitting to the vibrational energy level structure, particularly since the greatest deviation appears in the ground to first transition frequency.

Proton-Proton Motion. Next, we examine the ground state expectation values of the even moments of $(q-q_0)$ (Table 4). The first of these quantities is related to fluctuations in the dipole moment and all play a role in the rotation constants.

Table 4

Ground State Even Moments of $(q-q_0)$

<u>Moment</u>	<u>Correlated Bender</u>
$(q-q_0)^2$	0.910×10^{-2}
$(q-q_0)^4$	0.250×10^{-3}
$(q-q_0)^6$	0.114×10^{-4}
$(q-q_0)^8$	0.721×10^{-6}
$(q-q_0)^{10}$	0.578×10^{-7}

Rotational Constants. It is well known that the rotational level structure within a given band is determined by the rotational constant matrix. In Table 5 we display the A, B, and C rotational constant matrices that are obtained from a correlated bender model of H_2O . Finally, in Table 6 we display the measured experimental values for the diagonal elements of the A, B and C rotational constants (ref. 6).

A very interesting feature of this state is that both the A and B rotational constants increase relative to the ground state. Now, on naive grounds one might expect that as the molecule opens up (i.e., the bond angle increases) the B-rotational constant should decrease. The fact that it does not is indicative of a correlation between the ground state

Table 5

Rotational Constant Matrix for Correlated Bender

<u>A Rotation Constants =</u>			
0	27.876	-6.358	2.504
1	-6.358	31.470	-11.167
2	2.504	-11.167	36.394
<u>B Rotation Constants =</u>			
0	14.510	1.781	0.227
1	1.781	14.837	2.632
2	0.227	2.632	15.136
<u>C Rotation Constants =</u>			
0	9.297	0.084	-0.009
1	0.084	9.284	0.143
2	-0.009	0.143	9.214

Table 6

Experimental Rotation Constants

<u>A Rotation Constant</u>		<u>B Rotation Constant</u>		<u>C Rotation Constant</u>	
27.876	--	14.512	--	9.285	--
--	31.12	--	14.66	--	9.15

OH stretch mode and the first excited bending mode. This interpretation is underscored by our calculation. Specifically, the correlated bender, which does include this type of correlation, predicts a larger B rotational constant, which is in agreement with experiment.

Next, we note that the strength of the rotational-vibrational interaction is set by the size of the off-diagonal matrix elements of the rotational constants. For example, from the correlated bender model we have for the A-rotational constant

$$\frac{\langle 0 | A | 1 \rangle}{\langle 0 | A | 0 \rangle} = 0.22 \qquad \frac{\langle 1 | A | 2 \rangle}{\langle 1 | A | 1 \rangle} = 0.36$$

where for the B constant,

$$\frac{\langle 0 | B | 1 \rangle}{\langle 0 | B | 0 \rangle} = 0.12 \qquad \frac{\langle 1 | B | 2 \rangle}{\langle 1 | B | 1 \rangle} = 0.18$$

and

$$\frac{\langle 0 | C | 1 \rangle}{\langle 0 | C | 0 \rangle} = 0.01 \qquad \frac{\langle 1 | C | 2 \rangle}{\langle 1 | C | 1 \rangle} = 0.02$$

for the C constant. Note the dramatic increase in these ratios as we go from the ground to the first excited state, which is to be expected as the molecule opens up and becomes less rigid.

Molecular Geometry. Finally, we examine the geometric structure that our models of the water molecule imply. We recall that the structure parameters are so chosen that the model reproduces the experimentally obtained ground state A and B rotational constants. We take the static bond angle (bond angle in the absence of zero point vibrations) and ground state bond angle from the relations

$$\theta_0 = 2 \sin^{-1} (q_0/2) \quad (17)$$

$$\langle 0|\theta|0\rangle = 2\langle 0|\sin^{-1} \frac{1}{2} q|0\rangle \quad (18)$$

In Table 7 we present predicted versus measured values for the bond length, bond angle, and θ_0 for the model. An examination of the data reveals that the correlated bender yields a static bond angle that lies within 0.05% of the experimental value. Furthermore, the equilibrium bond angle is within 0.09% of the measured value.

Table 7

Geometric Structure of Water

Parameter	Observed	Correlated Bender	Deviation (%)
r	0.972 Å	0.960 Å	0.31
$\langle \theta \rangle$	104.50°	104.41°	0.09
θ_0	103.9°	103.95°	0.05

We can also demonstrate that fluctuations of the moment of inertia, $I(\theta)$, associated with the bending motion are not significant. The size of this effect is set by the ratio

$$\left| \frac{\langle I(\theta) \rangle - I(\theta_0)}{\langle I(\theta) \rangle} \right| = 8 \times 10^{-4} .$$

This corresponds to an energy of 0.32 cm^{-1} (the ground state energy of H_2O is about 850 cm^{-1}) and does not represent a significant effect in the rotational-vibrational structure of the molecule. Finally the hydrogen-hydrogen separation for the correlated bender is 1.53 Å.

C. Rotational-Vibrational Structure of Water

As we discussed in Sections IIA and IIB, the rotational structure of the water molecule is dominated by centrifugal distortion. Since our model directly incorporates this feature of H_2O , an excellent test of its accuracy is the rotational-vibrational energy levels themselves. In this section, we present theoretical calculations through $J = 10$ of the ground and first excited bending mode states using our model of water. In general, we find that the correlated bender displays a reliable picture of water as its predicted energy levels lie quite close to experimental findings. Furthermore, to measure the significance of the off-diagonal rotational constant matrix elements, we also present predicted rotational energies for a model in which these matrix elements have been set equal to zero. We note that these matrix elements represent the coupling between the various vibrational states and is a measure of the importance of centrifugal distortion on the structure of the molecule. These energies can be regarded as rigid rotor energies despite the fact that the rotational constants are given by the reciprocal moment of inertia tensor averaged over the ground or first vibrational state.

In Table 8 we display the predicted rotational-vibrational level structure in the ground vibrational state through $J = 10$ (ref. 7). As we are specifically interested in the effects of centrifugal distortion on the structure of the molecule, we present only those states with $\tau \geq 0$. It is well known that such states involve rotation about the small moments of inertia (A and B). On physical grounds it is clear that the coupling between molecular rotation and vibration is strongest for these states. This feature is reflected in the predicted level structure.

Table 8

Comparison of Rotational-Vibrational Energy Levels in (000) State

J_r	Observed	Rigid Rotor	% Dev.	Correlated bender	% Dev.
1 ₁	42.37	42.38	0.00	42.37	0.00
2 ₀	95.18	95.20	0.02	95.21	0.03
2 ₂	136.16	136.53	0.28	136.18	0.01
3 ₀	206.30	206.69	0.33	206.48	0.09
3 ₃	285.41	287.26	0.63	285.52	0.04
4 ₀	315.78	316.45	0.12	316.14	0.11
4 ₂	383.84	385.79	0.51	384.36	0.14
4 ₄	488.13	494.49	1.30	488.48	0.07
5 ₀	503.97	506.17	0.44	505.02	0.21
5 ₃	610.34	616.49	1.00	611.58	0.20
5 ₅	742.07	757.39	2.06	743.04	0.13
6 ₀	661.55	664.80	0.49	663.14	0.24
6 ₂	757.78	764.17	0.84	760.08	0.50
6 ₄	888.63	903.43	1.67	891.24	0.29
6 ₆	1045.06	1076.03	2.96	1047.30	0.21
7 ₀	927.75	935.07	0.79	931.30	0.38
7 ₃	1059.83	1074.59	1.39	1064.10	0.40
7 ₅	1216.19	1246.28	2.47	1221.05	0.40
7 ₇	1394.81	1450.41	3.99	1399.37	0.32
8 ₀	1131.77	1141.54	0.86	1136.57	0.42
8 ₄	1411.63	1441.61	2.13	1419.30	0.56
8 ₈	1789.12	1880.52	5.67	1797.40	0.46
9 ₀	1476.99	1493.33	1.11	1484.00	0.47
9 ₅	1810.59	1864.32	2.89	1823.60	0.72
9 ₇	2010.0	2099.19	4.43	2023.88	0.69
9 ₉	2225.55	2366.37	6.33	2239.60	0.63
10 ₀	1724.71	1747.54	1.32	1736.16	0.66
10 ₄	2054.37	2109.03	2.66	2072.37	0.88
10 ₆	2254.36	2342.81	3.92	2274.71	0.90
10 ₈	2471.59	2609.26	5.57	2493.26	0.88
10 ₁₀	2702.09	2907.95	7.62	2724.24	0.82

Specifically, an examination of Table 8 reveals that deviations between the model without centrifugal distortion and experiment increase drastically with increasing rotational energy. For example, the 9_0 and 10_0 states deviate from the experimentally derived values by only 1.11% and 1.32% whereas for the 9_9 and 10_{10} states, the deviation is 6.32% and 7.62%.

Next we consider the predicted level structure of the correlated bender. We first note that all values through $J = 10$ lie well within 1% of the experimental values. As some of these lie above the $(010) J = 0$ vibrational state, it is clear that this model presents an accurate picture of the structure of the molecule. To obtain a more detailed account of the model's success, we again examine centrifugal distortion. For the 8_3 state, the correlated bender accounts for 83.12 cm^{-1} or 90.9% of the effects of centrifugal distortion. Similarly, for the 10_{10} state, it accounts for 183.71 cm^{-1} or 89.2% of the energy. Thus, the correlated bender accounts for about 90% of the effects of centrifugal distortion in H_2O . In Table 9 we summarize these considerations for the important high energy states.

An examination of Table 9 reveals that the correlated bender accounts for 85 to 90% of the energy due to rotational distortion except for the anomalous states: 8_4 , 9_5 , 10_4 and 10_6 , i.e., the relatively low τ states. To account for this discrepancy, we note that we have not included Coriolis forces, which lead to energy changes that vary with the rotational state. Furthermore, this rotational-vibrational interaction enters into the molecular Hamiltonian by means of terms of the form $\sum_{\alpha} \xi_{\alpha} \pi_{\alpha}$. Rewriting this in a somewhat more transparent fashion,

$$H'_{\text{Cor}} = \vec{J} \cdot \vec{u} \cdot \vec{Q}_i \times \vec{P}_j$$

where μ can be approximated as a diagonal, rigid tensor for the sake of simplicity. Here \vec{Q}_i and \vec{P}_j refer to the vibrational modes. Since the bending mode involves the greatest deviation, we can take \vec{Q}_i to be parallel to the hydrogen-hydrogen separation. Taking \vec{P}_j as one of the OH stretch modes, it immediately follows that the component of \vec{J} that is parallel to the C-rotation axis is of greatest importance. However, \vec{J} is parallel to this axis only for the low τ states, and therefore it is these states that we describe most poorly with respect to the Coriolis interaction.

Table 9

Effects of Centrifugal Distortion

J_{τ}	Centrifugal Distortion	Correlated Bender	Amount
6 ₆	30.97	28.73	92.76
7 ₅	30.09	25.23	83.85
7 ₇	55.60	51.04	91.80
8 ₄	29.98	22.19	74.02
8 ₈	91.40	83.12	90.94
9 ₅	53.73	40.72	75.79
9 ₇	89.19	75.31	84.40
9 ₉	140.82	126.77	90.02
10 ₄	54.66	36.66	67.07
10 ₆	88.45	68.10	77.00
10 ₈	137.67	116.69	84.76
10 ₁₀	205.86	183.71	89.24

Finally, in Table 10 we have compared theory and experiment for rotational-vibrational levels that lie beyond $J = 10$. An examination of this table reveals that the model of a correlated bender accounts for these states within 1 to 1.5% accuracy. In view of the fact that we are

Table 10

Comparison of High-Energy Rotational-Vibrational Levels in (000) State

J_{τ}	Observed	Correlated Bender	% Dev.
11 ₀	2145.01	2161.74	0.87
11 ₅	2522.46	2549.74	1.08
11 ₉	2938.36	2973.07	1.18
11 ₁₁	3160.97	3216.60	1.76
12 ₀	2437.62	2460.86	0.95
12 ₂	2612.94	2642.63	1.14
12 ₄	2815.61	2848.67	1.25
13 ₀	2927.38	2965.20	1.22
13 ₃	3128.25	3171.36	1.38
13 ₅	3348.20	3398.26	1.50
13 ₇	3584.00	3640.19	1.57
14 ₋₆	2880.94	2900.34	0.67
14 ₋₂	3101.57	3135.81	1.04
14 ₀	3266.36	3309.54	1.32
15 ₋₈	3085.92	3111.93	0.91

dealing with a four parameter model that has been fit to only five pieces of data, the demonstrated accuracy is satisfying. Note that many of these rotational-vibrational states lie above 3000 cm^{-1} , which is about equal to the (020) state (ref. 8).

We note that the off-diagonal matrix elements of the rotation constants govern the coupling between the various vibrational states that arise from molecular rotation. Furthermore, these quantities cannot be directly measured and yield valuable information on the vibrational wave functions as they vary sensitively with the hydrogen-hydrogen motion. For example, for $\langle 0|A|1\rangle$ one has

$$\langle 0|A|1\rangle = C \int dq \psi_0(q) \frac{1}{1 - (q/2)^2} \psi_1(q) \quad (19)$$

where $\psi_0(\psi_1)$ is the ground [(010)] state vibrational wave function and C is a constant that does not concern us here. Note, that for $\langle 0|B|1\rangle$ one has

$$\langle 0|B|1\rangle = C \int dq \psi_0(q) \frac{1}{(q/2)^2} \psi_1(q) \quad (20)$$

Finally, in Table 11 we have compared theory and experiment for the (010) state. The overall accuracy for the correlated bender is on the order of 1 to 1.5% (ref. 9).

D. The Role of the Nuclear Masses

In this section we examine the significance of the nuclear masses in our correlated bender model of water. This is best done by investigating the rotational-vibrational spectra and structure of the symmetric isotopes

Table 11
 Comparison of Rotational-Vibrational Energy Levels in (010) State

J_{τ}	Observed	Correlated bender	Dev. %
1 ₁	45.89	46.41	1.13
2 ₀	99.03	100.26	1.24
2 ₂	149.05	150.77	1.15
3 ₀	219.28	222.23	1.35
3 ₃	313.01	316.52	1.12
4 ₀	328.45	332.85	1.34
4 ₂	411.53	416.70	1.26
4 ₄	535.01	539.77	0.89
5 ₀	531.85	539.48	0.68
5 ₃	657.08	664.91	1.19
5 ₅	811.65	816.83	0.64
6 ₀	687.97	687.48	0.07
6 ₂	804.68	814.82	1.26
6 ₄	959.39	969.77	0.98
6 ₆	1139.65	1144.59	0.43
7 ₀	975.07	989.82	1.51
7 ₃	1129.71	1143.95	1.26
7 ₅	1310.84	1321.98	0.85
7 ₇	1515.43	1520.38	0.33
8 ₀	1177.16	1196.23	1.62
8 ₄	1506.69	1524.39	1.17
8 ₈	1936.46	1941.97	0.28
9 ₀	1545.06	1570.72	1.66
9 ₅	1932.18	1944.05	1.13
9 ₇	2157.99	2173.90	0.74
9 ₉	2399.80	2406.75	0.29
10 ₀	1793.08	1825.12	1.79
10 ₄	2176.36	2207.98	1.45
10 ₆	2403.21	2430.62	1.14
10 ₈	2646.41	2667.14	0.78

D₂O and T₂O. Specifically, we present calculations of the A, B, and C rotation matrices as well as the rotational-vibrational energy levels. By comparing these results with H₂O a detailed picture of the role of the nuclear masses in the motion of the two hydrogen atoms can be obtained.

Before presenting these results, we first note that our effective potential $V(q)$ depends on the nuclear mass in two ways: (1) through the quantity

$$U = - \frac{\hbar^2}{2} \sum_{\alpha} \mu_{\alpha\alpha}$$

and (2) the correlated bender coordinate q . The dependence of the μ 's on the nuclear masses is obvious and need not be discussed in detail here, although we will present an order of magnitude estimate of its mass-dependence below. On the other hand, the dependence of q on the nuclear mass is interesting and characteristic of the technique we are using to model water and therefore must be discussed. We begin by noting that for any model of water, q corresponds to a one-dimensional path through the potential energy surface of the molecule. This path may be either linear or curved. For the rigid bender, q is merely the bending coordinate itself and can be identified with the bending mode axis (see Fig. 1). On the other hand, in the correlated bender model of water, q represents a curved path such as that displayed schematically in Figure 2. The degree in which this coordinate departs from a straight line parallel to the bending mode axis depends on the correlation between the bending mode and the OH stretch modes.

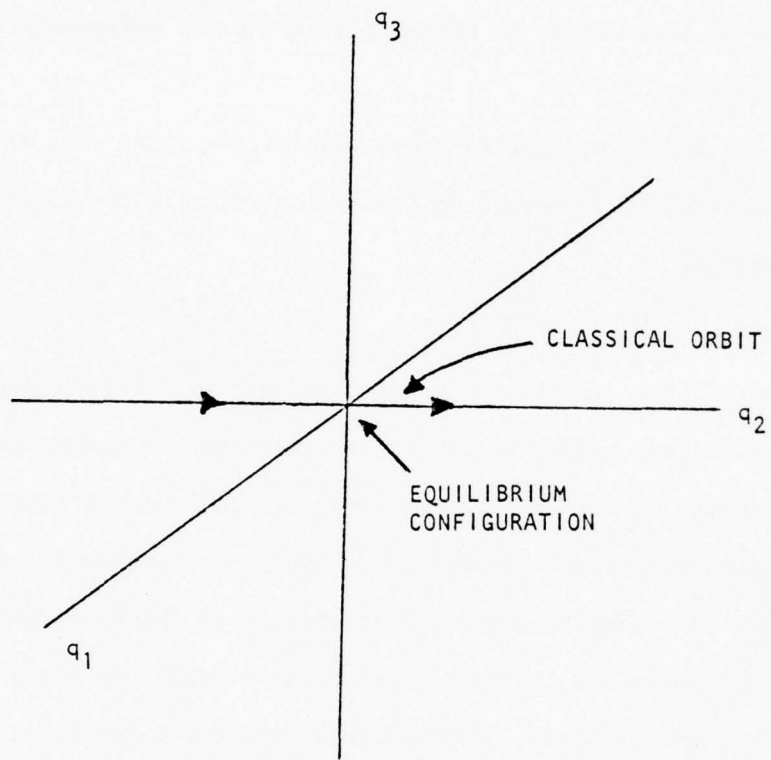


Figure 1. q coincides with the bending mode coordinate in the case of a rigid bender.

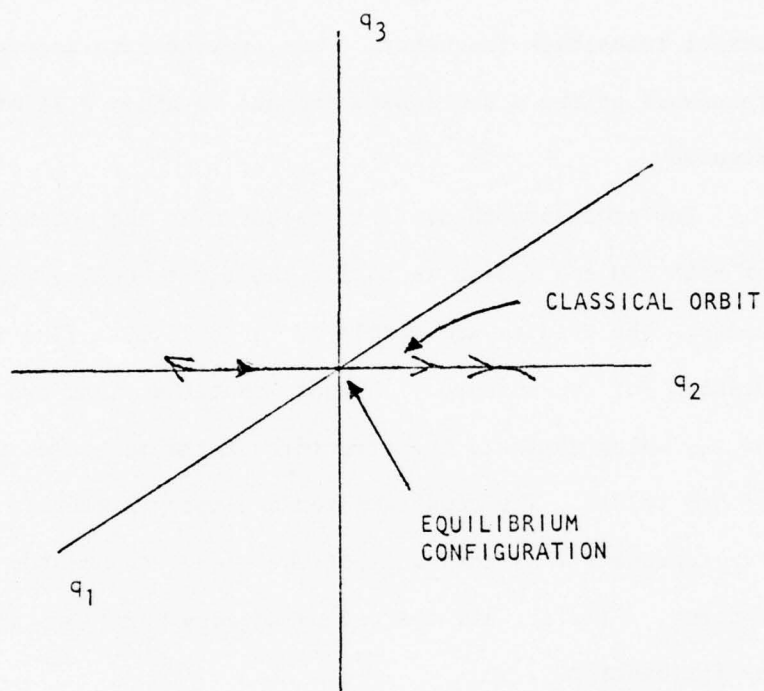


Figure 2. q is regarded as a curvilinear path through the potential energy surface of the molecule for the case of a correlated bender.

To estimate the contribution of the first effect we again use the rigid bender model as a test. Specifically, we apply the nuclear potential energy $V(q)$ generated in Section IIB for H_2O and calculate the first transition frequency of D_2O . We find a deviation of -11 cm^{-1} from the correct transition frequency. Thus, taking into account U , the mass dependence of the q coordinate amounts to about 0.5% of the transition frequency.

Our procedure then, is to redetermine the potential energy function for both D_2O and T_2O so as to fit the first bending mode transition frequency. The results are displayed in Table 12. (The results for H_2O are included for convenience.) We note that the first two terms, i.e., a_2 and a_4 , which dominate the structure of the molecule, vary by 1% from the H_2O to D_2O . The remaining terms display a greater variation; however, they represent less than 0.1% of the energy associated with the a_2 and a_4 terms. Finally, all the odd parameters were zero and v_2 transition was fit exactly.

Next, we examine the various rotation matrices. As the rotation-vibration interaction is manifested in the off-diagonal components of the rotation matrices, we confine our attention to these terms. Specifically, we examine the various ratios A_{ij}/A_{ii} , B_{ij}/B_{ii} , and C_{ij}/C_{ii} , where

$$A_{ij} \equiv |\langle i|A|j\rangle|$$

which are displayed in Table 13.

Table 12

Potential Energy Constants Display [cm^{-1}]

Parameter	H_2O	D_2O	T_2O
a_2	45510	46610	46590
a_4	-30835	-32580	-32147
a_6	-23665	-20508	-15002
a_8	1820	-26568	-22736

Table 13

Rotation Matrices

Parameter	H_2O	D_2O	T_2O
A_{01}/A_{00}	0.22	0.19	0.17
A_{02}/A_{00}	0.09	0.06	0.05
A_{12}/A_{11}	0.35	0.28	0.25
B_{01}/B_{00}	0.12	0.10	0.09
B_{02}/B_{00}	0.02	0.01	0.01
B_{12}/B_{11}	0.18	0.15	0.15
C_{01}/C_{00}	0.01	0.01	0.01
C_{02}/C_{00}	~0	~0	~0
C_{12}/C_{11}	0.02	0.02	0.02

An examination of Table 13 reveals that there is a systematic trend, in particular, the corresponding off-diagonal matrix elements of H₂O, D₂O, and T₂O all decrease with increases in the nuclear masses. Furthermore, these decreases are systematic, as each successive molecule decreases by 80%, i.e.,

$$(A_{01}/A_{00})_{T_2O} \sim 0.8(A_{01}/A_{00})_{D_2O} \sim 0.64(A_{01}/A_{00})_{H_2O}.$$

Finally, in Table 14 we compare theory and experiment for 10 rotational-vibrational energy levels in the ground and (010) excited vibrational states. In general, agreement with the experimentally derived values is on the order of 0.6%, which is satisfactory in view of the fact the only experimental data used in constructing this model of D₂O were the first transition frequency (i.e., ν_2) and the A and B ground state rotation constants (ref. 9).

Table 14

Rotational-Vibrational Energy Level Structure in D₂O [cm⁻¹]

ν	J_{τ}	Observed	Theory	% Dev.
0	10 ₀	908.19	911.83	+0.40
0	10 ₂	1002.85	1007.65	+0.47
0	10 ₄	1114.85	1120.84	+0.53
1	10 ₄	1166.85	1177.64	+0.92
0	10 ₆	1241.93	1249.16	+0.57
1	10 ₆	1307.67	1317.18	+0.80
0	10 ₈	1382.69	1390.97	+0.60
1	10 ₈	1464.2	1470.2	+0.41
0	10 ₁₀	1535.84	1545.14	+0.60
1	10 ₁₀	1636.79	1635.11	-0.10

SECTION III

A PREDICTIVE PHENOMENOLOGICAL MODEL OF WATER VAPOR

As we have discussed in earlier sections of this report, centrifugal distortion dominates the rotational-vibrational level structure of light asymmetric molecules. For such molecular systems, only the lowest rotational states can be described within the confines of a rigid rotor model. Higher rotational states are strongly coupled to the vibrational degrees of freedom, and nonrigid effects become an important component of the molecule's internal structure. For example, in water vapor, the rigid rotor approximation breaks down by $J = 4$, and one must include centrifugal distortion within some well justified scheme.

From the discussion presented above, it is clear that if one wishes to characterize the high-resolution infrared spectral data that are available for such molecular systems, a scheme that readily incorporates non-rigid effects must be employed. One such approach is the Watson rotational Hamiltonian, which is a series expansion in the various components of the molecular angular momentum. This is essentially a perturbative approach that is beset with a number of difficulties that render it inappropriate for current Air Force needs.

In this section, we outlined a new phenomenological approach to centrifugal distortion in light asymmetric molecules, particularly H_2O . This technique does not involve a series expansion in powers of the angular momentum; instead it is based on the notion of fitting the full rotational matrix (diagonal and off-diagonal components) to the spectral data. Our approach, which is nonperturbative in nature, has the additional advantage

that the phenomenological parameters obtained to characterize the spectrum are related to the potential energy surface of the molecule in a straightforward fashion. Furthermore, as we shall explicitly demonstrate, our method is predictive in the sense that it will determine the position of rotational levels that lie far above those used in the fitting scheme. Finally, as we shall discuss in Section III E, our technique offers the possibility of constructing highly accurate potential energy surfaces extending over regions of many thousands of wave numbers. This in turn will enable us to construct spectroscopically accurate transition dipole moment matrix elements that are required for a complete description of the absorption spectrum.

A. Theoretical Foundation

For simplicity, we shall confine ourselves to symmetrical nonlinear molecules, in particular H_2O , in which the reciprocal moment of inertia tensor is diagonal; i.e., $\mu_{\alpha\beta} = \delta_{\alpha\beta} \mu_{\alpha\alpha}$. Furthermore, we shall suppose that both Coriolis forces as well as vibrational angular momentum are of little significance and can be neglected. In that case, the Hamiltonian reduces to

$$H = \frac{1}{2} \sum_{\alpha} \Pi_{\alpha} \mu_{\alpha\alpha} \Pi_{\alpha} + \frac{1}{2} \sum_k P_k^2 + V \quad (20)$$

For situations in which one cannot neglect the effects of vibrational angular momentum or Coriolis forces, our method can be suitably extended. We defer discussion on the point until the end of this section.

We can best display our approach by first outlining the usual technique that one uses to solve equation (20). Let $|k_1, \dots\rangle$ and $\epsilon_{k_1, \dots}$ be

the eigenvectors and eigenvalues when the molecule is in the state $J = 0$, but with vibrational quantum numbers (k_1, \dots) . We emphasize that these eigenstates are unknown to us, as is the potential V . We shall assume, however, that the vibrational energy levels $\epsilon_{k_1, \dots}$ are known. If the molecule is rotating, centrifugal distortion will give rise to a coupling between the different vibrational eigenstates. As a consequence, the rotational-vibrational wave function can be written as

$$|J \tau M_J, n_1, \dots\rangle = \sum_K \sum_{k_1} C_{K, k_1, \dots}^{J, \tau, n_1, \dots} |k_1, \dots\rangle \times |JKM_J\rangle \quad (21)$$

where $|JKM_J\rangle$ are the rigid symmetric rotor wave functions and the expansion

coefficients $C_{K, k_1, \dots}^{J, \tau, n_1, \dots}$ are obtained from a matrix diagonalization.

The energy associated with the eigenstate (21) is

$$E_{J, \tau, n_1, \dots} = \epsilon_{n_1, \dots} + \sum_{\alpha KK'} C_{K, k_1, \dots}^{J, \tau, n_1, \dots} C_{K', k'_1, \dots}^{J, \tau, n'_1, \dots} \langle JK | \pi_\alpha^2 | JK' \rangle \langle k_1, \dots | u_{\alpha\alpha} | k'_1, \dots \rangle \quad (22)$$

where the matrix elements $\langle JK | \pi_\alpha^2 | JK' \rangle$ are fully tabulated. Equations (21) and (22) represent a complete quantum mechanical solution to the Hamiltonian (20), and demand that the intranuclear potential energy surface V be known. In general, this is not the case. Instead, observed spectral data yield the eigenenergies $E_{J, \tau, n_1, \dots}$ (and $\epsilon_{n_1, \dots}$). We now wish to examine Equation (22) as a means of cataloging spectral lines as well as deducing a potential energy surface V . To this end, we note that the

only unknown quantities that appear in (22) are the matrix elements of the inverse of the moment of inertia tensor, i.e., $\langle k_1, \dots | \mu_{\alpha\alpha} | k'_1, \dots \rangle$. These matrix elements along with $\langle JK | \pi_{\alpha}^2 | JK' \rangle$ appear in the Hamiltonian matrix that is diagonalized to obtain the $E_{J\tau; n_1, \dots}$. On the other hand all matrix elements of the vibrational Hamiltonian H_V are

$$\langle K_1, \dots | H_V | k'_1, \dots \rangle = \epsilon_{k_1, \dots} \delta_{k_1 k'_1} \dots$$

so that only a knowledge of the vibrational energy spacings, etc., is required. Of greatest importance are the quantities $\langle k_1, \dots | \mu_{\alpha\alpha} | k_1, \dots \rangle$. This suggests an interesting and practical approach to generating high-resolution line spectra for molecular systems. In particular, we propose to use the observed spectral line data to obtain the diagonal and off-diagonal matrix elements of $\mu_{\alpha\alpha}$ by a least squares fitting procedure. As noted above, matrix diagonalization yields the required coefficients

$J_{\tau, n_1, \dots}$
 $C_{K, k_1, \dots}$. Using Equation (22), we can catalog the rotational-vibrational

energy levels, and in addition, predict many new high-lying states that are not used in the fitting scheme. This point will be explicitly demonstrated below. Before discussing simplifying approximations that can be used in the above scheme, we first note that the diagonal matrix elements of the $\mu_{\alpha\alpha}$ are simply related to the various molecular rotation constants that are often known. This can reduce the number of unknown parameters required for describing the spectrum. We note that the off-diagonal matrix elements are not directly observable.

Next, we determine the effect of the various matrix elements of the $\mu_{\alpha\alpha}$ on a given rotational-vibrational band. This is essential if we are

to make any simplifying approximations. Suppose we are interested in the rotational level structure of a particular vibrational band labeled by the quantum numbers k_1, \dots . Then, the effect of the level labeled by k'_1, \dots is set by the following parameter

$$\eta \lesssim J(J+1) \frac{\langle k_1, \dots | \mu_{\alpha\alpha} | k'_1, \dots \rangle}{\epsilon_{k_1, \dots} - \epsilon_{k'_1, \dots}} < \frac{E_{J\tau, k_1, \dots} - \epsilon_{k_1, \dots}}{\epsilon_{k_1, \dots} - \epsilon_{k'_1, \dots}}$$

which is equal to the ratio of the rotational energy divided by the vibrational spacings between the two levels. It follows then that near-lying vibrational levels have a strong influence on the structure of the rotational positions. Thus, a Fermi resonance, such as exists between the (100) and (020) states of water will be of extreme importance. On the other hand, distant states will have a negligible effect, and, if desired, can be ignored.

B. Comparison to Other Approaches

At the present time there exists a number of other approaches for calculating and characterizing molecular spectral line data. These are listed below.

1. Using the Born-Oppenheimer approximation, calculate the intranuclear potential energy surface. Following this, one then solves the Schrödinger equation for a rotating-vibrating molecule to obtain the system's level structure and wave functions.
2. Construct a phenomenological potential energy surface from experimentally deduced vibrational spacings and rotation constants. Following this, one then solves the Schrödinger wave equation for the rotational-vibrational level structure and eigenfunctions.

3. The phenomenological Watson Hamiltonian

$$\begin{aligned}
 H_W = & \frac{1}{2}(B+C)J^2 + A - \frac{1}{2}(B+C) (J_z^2 - b_p J_z^2) \\
 & - \Delta_J J^4 - \Delta_{JK} J^2 J_z^2 - \Delta_K J_z^4 - 2\delta_J J^2 J_z^2 - \delta_K (J_z^2 J_z^2 + J_z^2 J_z^2) \\
 & + H_J J^6 + H_{JK} J^4 J_z^2 + H_{KJ} J^2 J_z^4 + H_K J_z^6 + 2h_J J^4 J_z^2 \\
 & + h_{JK} J^2 (J_z^2 J_z^2 + J_z^2 J_z^2) + h_K (J_z^4 J_z^2 + J_z^2 J_z^4) + L_{JK} J^4 J_z^4 \\
 & + L_K J_z^3 + 2\lambda_J J^6 J_z^2 + \lambda_{JK} J^4 (J_z^2 J_z^2 + J_z^2 J_z^2) + P_{KJ} J^4 J_z^6 \\
 & + P_K J_z^{10} + P_{KKJ} J^2 (J_z^6 J_z^2 + J_z^2 J_z^6)
 \end{aligned}$$

is fitted to the observed rotational spectrum of water for a specific vibrational band. The various coefficients A, B, C, Δ_J , ... P, P_{KKJ} vary in a striking manner from vibrational state to vibrational state. As a consequence, one must re-do the fitting procedure for different spectral regions.

The first approach, although first principles in nature, is limited to accuracies on the order of 0.1 eV; i.e., several hundred wave numbers. Hence, it cannot be used for high-resolution work. Furthermore, the computer time for such projects is truly enormous, and in terms of cost effectiveness, is totally inappropriate. Finally, such first principles studies take much too long for Air Force needs.

We have used the second approach successfully to model the CO₂, CO, and DF regions of the water vapor spectrum in Section IV. In general, such a technique yields a predictive, reliable model of water, which yields levels that are accurate to about 0.1 cm⁻¹. Such a model yields

much useful information on water vapor absorption. However, for ultra-high resolution studies that are currently required, they must be replaced by a somewhat more phenomenological model. As we shall discuss in Section IIID, the present approach that we will use for HF can be regarded as a first generation descendant of the second technique.

The third approach is totally unsuitable for Kirtland's needs. The reasons for this have been discussed in a previous technical report (ref. 10).

C. Preliminary Results on the Bending Mode Vibrational Bands

In this section we present some preliminary results that illustrate our technique. These results can be considerably improved with new iterative techniques that we will incorporate into our programs. Furthermore, this work did not include enough of the vibrational states. Despite this, our results are impressive. In particular, we are concerned with the ground, (010), and (020) rotational-vibrational bands of water vapor. Accordingly, we have least squares fit the various rotational matrix elements to a total of 72 rotational levels that lie within these bands. The specific states used in the fitting scheme are exhibited in Table 15, along with the associated energies and deviations. In obtaining this fit, our Hamiltonian matrix covered the space spanned by the following six vibrational states: (000), (010), (020), (030), (100), and (110). We emphasize that rotational data from only the first three of these bands was used. Since the rotation matrix elements are all symmetric, in the sense that

$$\langle k_1, \dots | \mu_{\alpha\alpha} | k_1', \dots \rangle = \langle k_1', \dots | \mu_{\alpha\alpha} | k_1, \dots \rangle$$

there are 65 rotation constants that enter into the problem. As the ground and first excited diagonal elements are already known, this leaves 57 parameters to be chosen to least squares fit 72 rotational levels. As we shall see, most of these are not significant.

An examination of Table 15 reveals that our fitting procedure was successful, especially in view of the severe limitations placed on the states used and the fact that the Coriolis force was not included. We feel that this is adequate considering the fact that we are fitting to three different bands with energies up to 5403 cm^{-1} . The fit could be considerably improved (especially with regard to the (020) state) by including the following vibrational states in our Hilbert space: (040), (200), (002), (120). (Note, it is not necessary to have the level values for these states.)

Next, we demonstrate that our technique is predictive in the sense that it yields the correct rotational levels for states that lie well beyond those used for fitting purposes. In Table 16, we have displayed the predicted versus observed rotational levels for states that lie at $J = 10$ and higher in the ground, (010), and (020) vibrational states. Typical accuracies range from 0.01% to 1% of the rotational energy. Note that many of the levels in the ground vibrational state have rotational energies that are greater than 3000 cm^{-1} and therefore will couple strongly to the (020) state. Furthermore, the predicted results for the (020) state are excellent. In particular, the 12_5 level has a rotational energy of 2242 cm^{-1} , and the predicted level position deviated by only 0.2% of the experimental value. To our knowledge, there does not exist a single theory that accounts for all of these states as well as that presented here.

Table 15

Comparison of Observed and Calculated
Rotational-Vibrational Energy Levels

<u>V</u>	<u>J</u>	<u>τ</u>	<u>Obs.</u> <u>(cm^{-1})</u>	<u>Cal.</u> <u>(cm^{-1})</u>	<u>Dev.</u> <u>(cm^{-1})</u>	<u>V</u>	<u>J</u>	<u>τ</u>	<u>Obs.</u> <u>(cm^{-1})</u>	<u>Cal.</u> <u>(cm^{-1})</u>	<u>Dev.</u> <u>(cm^{-1})</u>
0	1	-1	23.79	23.79	0.00	1	7	-5	2309.89	2311.72	1.83
0	1	0	37.14	37.13	0.01	1	7	-3	2392.38	2392.79	0.41
0	1	1	42.37	42.37	0.00	1	7	-1	2462.87	2460.84	2.03
1	1	-1	1618.41	1618.40	0.01	1	7	3	2724.30	2724.41	0.11
1	1	0	1634.93	1634.83	0.01	1	7	5	2905.43	2909.72	4.29
1	1	1	1640.48	1640.41	0.07	2	7	-7	3738.60	3738.54	0.06
2	1	-1	3175.44	3175.56	0.12	2	7	-5	3879.34	3880.25	0.91
0	3	-3	136.76	136.72	0.04	2	7	-3	3967.48	3969.34	1.86
0	3	0	206.30	206.35	0.05	2	7	-1	4052.83	4052.01	0.82
0	3	3	285.41	285.72	0.31	2	7	3	4368.64	4364.87	3.77
1	3	-3	1731.92	1731.92	0.00	2	7	5	4578.97	4575.27	3.70
1	3	0	1813.87	1813.62	0.25	0	9	-7	1079.07	1077.49	1.60
1	3	3	1907.71	1908.35	0.84	0	9	-5	1201.91	1201.64	0.27
2	3	-3	3289.24	3289.61	0.37	0	9	-3	1282.91	1282.68	0.23
2	3	0	3387.68	3384.37	3.27	0	9	1	1477.29	1477.36	0.07
0	5	-5	325.34	324.96	0.40	0	9	3	1631.38	1632.11	0.73
0	5	0	503.97	504.15	0.18	0	9	5	2009.83	2008.79	1.09
0	5	5	742.07	743.74	1.67	1	9	-9	2512.37	2511.41	0.96
1	5	-5	1920.70	1921.14	0.44	1	9	-5	2818.40	2822.53	4.13
1	5	0	2126.44	2125.93	0.51	1	9	-3	2904.82	2904.38	0.44
2	5	-5	3478.98	3479.19	0.21	1	9	3	3321.1	3318.9	2.2
2	5	0	3719.50	3718.51	1.01	1	9	6	3752.58	3752.53	0.05
0	7	-3	782.41	782.42	0.01	1	9	9	3994.59	3988.60	5.99
0	7	-1	842.35	842.29	0.06	2	9	-9	4068.70	4067.44	1.26
0	7	3	1059.83	1060.88	1.05	2	9	-7	4263.14	4263.76	0.62
0	7	5	1216.19	1218.13	1.94	2	9	-3	4493.81	4496.23	2.42
0	7	7	1394.81	1397.07	2.26	2	9	1	4784.67	4782.28	2.39
1	7	-7	2180.68	2180.94	0.26	2	9	3	4992.14	4995.10	2.96
						2	9	6	5483.34	5481.96	1.38

Table 16
Comparison of High-Lying Levels to Experiment

<u>V</u>	<u>J</u>	<u>τ</u>	<u>Obs. (cm^{-1})</u>	<u>Cal. (cm^{-1})</u>	<u>Dev. (cm^{-1})</u>	<u>V.</u>	<u>J</u>	<u>τ</u>	<u>Obs. (cm^{-1})</u>	<u>Cal. (cm^{-1})</u>	<u>Dev. (cm^{-1})</u>
0	10	-6	1437.19	1437.19	0.78	0	14	2	3465.4	3457.06	8.34
0	10	-2	1616.45	1615.73	0.72	0	15	-8	3083.92	3077.23	6.59
0	10	2	1875.45	1874.94	0.51	1	10	-6	3058.6	3065.49	6.89
0	10	6	2254.36	2252.23	2.12	1	10	-2	3253.91	3250.65	3.26
0	10	10	2702.09	2682.14	19.95	1	10	2	3565.3	3560.52	4.78
0	11	-5	1813.47	1812.64	0.83	1	10	6	3997.8	3993.27	4.53
0	11	-3	1899.21	1898.01	1.20	1	10	8	4241.0	4230.98	10.02
0	11	1	2144.46	2142.98	1.48	1	11	-5	3323.55	3322.38	8.83
0	11	5	2522.46	2519.04	3.42	1	11	-3	3487.59	3491.54	4.05
0	12	-6	2105.87	2104.76	1.11	1	11	1	3660.2	3654.9	5.3
0	12	-2	2300.67	2298.61	2.06	1	11	5	4266.05	4257.96	3.09
0	12	2	2612.94	2610.54	2.40	2	10	-10	4260.36	4256.98	3.38
0	12	4	2813.61	2808.95	4.66	2	10	-8	4480.39	4480.87	0.48
0	13	-7	2413.95	2412.62	1.33	2	10	-4	4752.74	4755.71	2.97
0	13	-4	2586.5	2584.09	2.41	2	10	0	5030.04	5033.44	3.40
0	13	+0	2927.38	2923.83	3.55	2	10	2	5237.79	5240.42	2.63
0	13	3	3128.25	3121.70	6.55	2	11	9	4714.82	4715.96	1.14
0	13	5	3348.2	3336.15	12.05	2	11	-7	4905.64	4909.35	3.71
0	14	-7	2745.5	2741.67	3.83	2	11	-5	5034.39	5038.95	4.56
0	14	-3	3085.0	3080.59	4.41	2	11	-3	5144.41	5141.65	2.76
0	14	+0	3266.36	3260.62	5.74	2	12	-10	4966.64	4965.09	0.55
						2	12	-5	5388.97	5393.59	4.62

The least squares fitting of the rotational constant matrix elements to obtain rotational-vibrational levels for ground, (010) and (020) states matrix diagonalization automatically yields the energy level structure for other bands. It is of interest then to compare these values to experiment. In Table 17, we have displayed the predicted versus the experimental values for the low-lying rotational levels in the (110) state. We emphasize that outside of the vibrational spacings of these states, no experimental information was used. Finally, in Tables 18 through 20 we have compared predicted versus experimental frequencies in the CO₂, CO, and DF regions. In Table 21 results for the 001 band are exhibited.

D. Present Data Base, Vibrational Bands of Significance for HF Transitions, and an Iterative Data Link

At the present time there exists a number of sources of data on water vapor transitions. By far, the most accurate are those of Rao (ref. 7) and Gordy's group (ref. 6). Other data bases include Hall and Dowling (ref. 9), and Benedict (ref. 11). Rao's results include rotational states through $J = 15$ for the following vibrational bands: (000), (020), (100), (001), (011), (110), and (030). Level positions are reported to an accuracy of 10^{-2} cm⁻¹ and are extensive. No data were reported with respect to the (010) vibrational band by this group. Nevertheless, level positions of 10^{-2} cm⁻¹ are available.

HF transitions occur from 2 to 5 μ m, i.e., they span the spectrum from about 3000 to 500 cm⁻¹. The following vibrational bands are of interest: (1) ground; (2) ν_2 ; (3) $2\nu_2$; (4) $3\nu_2$; (5) ν_1 ; (6) ν_3 ; (7) $\nu_2 + \nu_3$; and (8) $\nu_1 + \nu_2$. An examination of Benedict's ESSA tables reveals that rota-

tional states through $J = 15$ appear for the transitions involving ν_3 , $\nu_1 + \nu_2$ and $\nu_2 + \nu_3$, although the bulk are in the $J = 10, 11$ range.

Table 17
Comparison of Low-Lying Rotational-Vibrational
Levels in the (110) Bands

<u>V</u>	<u>J</u>	<u>τ</u>	<u>Obs.</u> <u>(cm^{-1})</u>	<u>Pred.</u> <u>(cm)</u>	<u>Dev.</u> <u>(cm^{-1})</u>	<u>% Dev.</u> <u>of rot.</u> <u>energy</u>
110	1	-1	5258.40	5258.42	0.02	0.09
110	1	0	5274.16	5274.12	0.04	0.1
110	1	1	5279.67	5279.38	0.29	0.6
110	2	-2	5304.01	5304.47	0.46	0.67
110	2	0	5332.01	5331.70	0.31	0.32
110	2	2	5379.95	5380.41	0.46	0.32

Table 18
Comparison of Model to Experiment for CO₂ Laser Wavelengths

LINE		Observed (cm ⁻¹)	Calculated	Deviation
Upper State	Lower State			
(0,1,0); 7 ₋₇	(0,0,0); 8 ₁	925.49	925.68	0.19
(0,1,0); 9 ₋₂	(0,0,0); 10 ₄	928.94	928.11	0.07
(0,1,0); 9 ₋₁	(0,0,0); 10 ₃	944.33	944.45	0.07
(0,1,0); 8 ₀	(0,0,0); 9 ₄	961.08	964.5	2.42
(0,1,0); 10 ₋₁₀	(0,0,0); 10 ₀	980.4	980.92	0.52
(0,1,0); 9 ₋₉	(0,0,0); 9 ₁	1035.14	1035.86	0.03
(0,1,0); 10 ₆	(0,0,0); 9 ₋₄	1038.07	1042.37	4.30
(0,1,0); 9 ₋₈	(0,0,0); 10 ₋₆	1072.19	1072.41	0.22
(0,1,0); 8 ₋₇	(0,0,0); 9 ₋₅	1076.88	1077.57	0.69
(0,1,0); 10 ₋₇	(0,0,0); 11 ₋₅	1091.24	1093.67	2.43
(0,2,0); 7 ₋₇	(0,1,0); 8 ₋₃	1108.38	1108.73	0.35
(0,2,0); 4 ₋₃	(0,1,0); 5 ₃	1129.87	1130.31	0.44
(0,2,0); 6 ₋₄	(0,1,0); 7 ₀	1143.54	1145.86	1.82
(0,0,0); 12 ₄	(0,1,0); 12 ₋₆	1118.56	1122.39	3.83

Table 19
Comparison of Model to Experiment at CO Laser Wavelengths

LINE				
<u>Upper State</u>	<u>Lower State</u>	<u>Observed</u>	<u>Calculated</u>	<u>Deviation</u>
(0,0,1); 9 ₋₆	(0,1,0); 10 ₋₇	1913.24	1913.75	0.51
(0,2,0); 7 ₀	(0,1,0); 6 ₀	1903.87	1904.18	0.31
(0,0,1); 8 ₋₄	(0,1,0); 9 ₋₅	1906.65	1909.37	2.72
(0,2,0); 5 ₀	(0,1,0); 4 ₃	1920.85	1921.38	0.53
(0,1,0); 10 ₋₂	(0,0,0); 11 ₋₁₁	1926.63	1929.62	2.99
(0,0,1); 11 ₋₁₁	(0,1,0); 12 ₋₁₂	1917.4	1919.41	2.01
(0,1,0); 6 ₋₁	(0,0,0); 5 ₋₅	1946.35	1947.94	1.59
(0,1,0); 7 ₃	(0,0,0); 6 ₁	1957.01	1957.08	0.07
(0,0,1); 5 ₁	(0,1,0); 6 ₀	1965.59	1969.45	3.86
(0,0,1); 8 ₆	(0,1,0); 8 ₅	1983.71	1985.75	2.04
(0,0,1); 5 ₋₂	(0,1,0); 6 ₋₃	2004.17	2005.75	1.58
(0,0,1); 8 ₋₅	(0,1,0); 8 ₋₂	2070.24	2071.69	1.45
(0,2,0); 8 ₆	(0,1,0); 7 ₄	2103.08	2106.67	3.59
(0,0,1); 3 ₂	(0,1,0); 3 ₃	2122.44	2123.14	0.70
(0,0,1); 2 ₋₂	(0,1,0); 1 ₋₁	2206.67	2206.67	0.0
(0,1,0); 9 ₃	(0,0,0); 9 ₋₇	2241.93	2242.53	0.6
(0,0,1); 8 ₋₃	(0,1,0); 7 ₋₄	2301.06	2301.63	0.57

Table 20
Comparison of Model to Experiment in the DF Region

<u>Upper Level</u>	<u>Lower Level</u>	<u>Observed</u>	<u>Calculated</u>	<u>Deviation</u>
(0,0,1); 7 ₋₂	(0,1,0); 6 ₋₅	2510.50	2512.83	2.33
(0,1,0); 14 ₋₁₀	(0,0,0); 13	2555.38	2559.81	4.43
(0,1,0); 10 ₈	(0,0,0); 9 ₂	2609.72	2618.72	9.0
(0,0,1); 8 ₋₄	(0,1,0); 7 ₋₇	2544.40	2547.13	2.73
(0,1,0); 10 ₄	(0,0,0); 9 ₋₆	2690.38	2687.48	2.9
(0,1,0); 11 ₃	(0,0,0); 9 ₋₇	2744.77	2746.37	4.4
(0,1,0); 11 ₅	(0,0,0); 11 ₋₉	2804.45	2812.45	8.0
(0,1,0); 9 ₄	(0,0,0); 8 ₋₄	2543.75	2545.76	2.1
(0,0,1); 7 ₀	(0,1,0); 6 ₋₃	2497.66	2496.38	1.28
(0,1,0); 10 ₄	(0,0,0); 9 ₋₆	2690.38	2694.58	4.2

Table 21
Rotational-Vibrational Level Structure for (001) State

J	τ	Observed energy (cm ⁻¹)	Calculated energy (cm ⁻¹)	Dev. (cm ⁻¹)
1	1	3796.98	3796.98	0.0
2	0	3849.38	3849.36	0.02
3	3	4030.51	4030.41	0.10
4	0	4066.11	4065.78	0.33
5	-3	4149.89	4150.08	0.19
5	3	4345.57	4345.49	0.08
6	-2	4350.70	4350.98	0.28
6	6	4759.85	4762.08	2.23
7	-5	4448.98	4448.85	0.13
7	1	4664.16	4663.18	0.02
7	5	4929.07	4928.44	0.63
8	-5	4625.94	4625.99	0.05
8	0	4861.80	4863.53	1.73
9	-9	4661.43	4660.52	0.91
9	0	5193.46	5194.05	0.59
9	6	5694.09	5693.28	0.81
10	-6	5171.05	5171.11	0.06
10	0	5442.09	5441.51	0.58
10	9	6355.63	6365.44	9.81
11	-11	5062.00	5060.52	1.48
11	-9	5255.23	5253.02	2.21

We envision the calculation of the HF transition lines to proceed as follows:

- (1) Initial values for the rotational constant matrices are taken from our old codes.
- (2) The rotational-vibrational spectral line structure is calculated and compared to existing data or new Kirtland data.
- (3) An iterative loop is set up in which the rotational matrices are varied until the best values for the spectral lines are obtained.
- (4) A Coriolis matrix is included to further refine the computed spectral lines.
- (5) A new iterative procedure is set up until the desired convergence is reached.

See Figure 3 for a flowchart of this procedure.

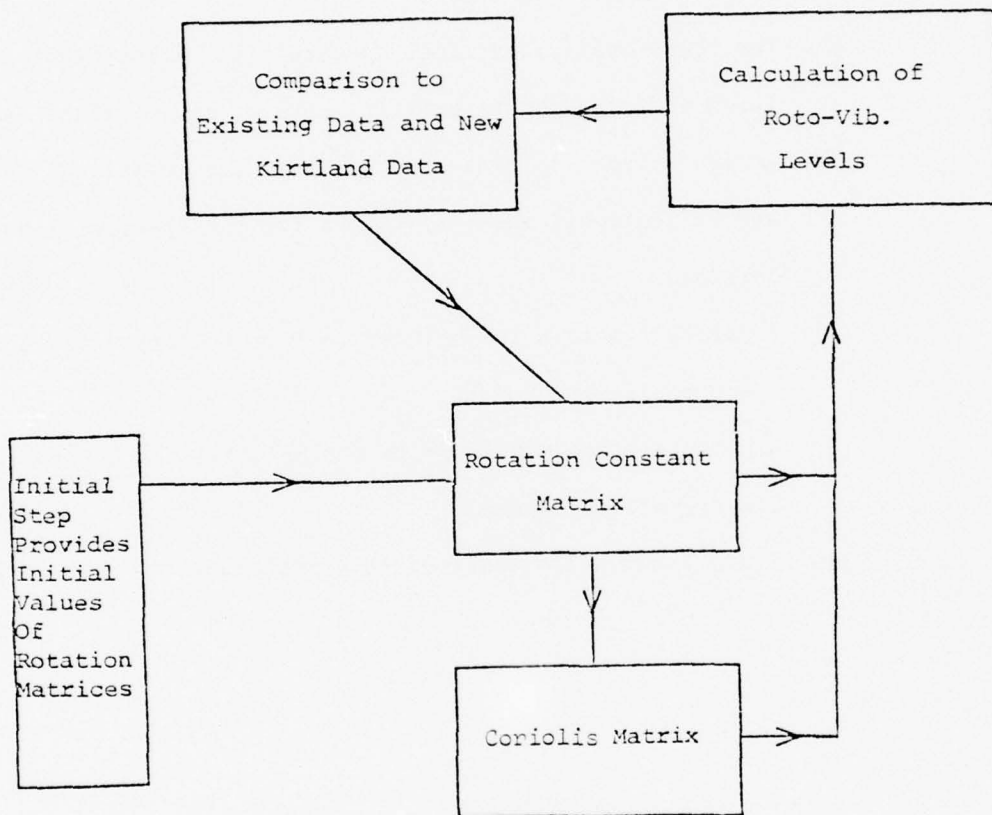


Figure 3. Flowchart for iterative calculation of HF transition lines.

E. Future Applications

In this section, we discuss the manner in which our water vapor model can be extended to obtain the detailed characteristics of the HF absorption region; i.e., line shape, line shift and line intensity. We first note that the line shape and line shift essentially arise from rotational quenching by means of long range multipole forces. Hence, these features of the absorption spectrum demand a detailed knowledge of the rotational wave functions as well as the multipole forces. The basic features of these forces can be obtained from classical electrodynamics and should not give rise to any difficulties. Furthermore, the rotational eigenfunctions are generated from our computer package and therefore pose no problem. In the event that quantum dispersion forces are significant, a suitable phenomenology can be developed.

Line intensities demand a knowledge of the transition dipole moment matrix elements between different vibrational states. Thus, a knowledge of the various vibrational wave functions, and therefore of the potential energy surface, is required. To this end, we note that the various rotation constant matrix elements are sensitive functions of the vibrational potential. For example, the diagonal and off-diagonal matrix elements of the A rotational matrix are given by

$$\begin{aligned} \langle k_1, k_2 | A | k_1', k_2' \rangle &= C \langle k_1 | \frac{1}{(1 + \sqrt{2}q_1 + q_1^2/2)} | k_1' \rangle \\ &\quad \langle k_2 | \frac{1}{\cos^2\theta} | k_2' \rangle \end{aligned}$$

where C is a known constant, q_1 is the dimensionless vibrational constant for the stretch mode, and θ is the bond angle. The fact that the A rotational constant varies so much from state to state implies that it depends strongly on the vibrational wave function and therefore is a sensitive probe of the potential energy surface. Furthermore, the large size of off-diagonal matrix elements such as $\langle 020 | A | 100 \rangle$ is a sensitive probe of mode-mode interaction pieces of the potential energy surface. Thus, by combining the various rotational constants generated by our fitting technique with the $J = 0$ vibrational energy level spacings, we should obtain a very complete picture of the potential energy surface and therefore of the vibrational wave functions.

Other molecular systems of interest that we feel can be approached by means of this technique are HDO, O_3 , N_2O and CH_4 .

SECTION IV
MULTIMODE MODEL OF THE WATER MOLECULE

In this section, we describe our multimode model of the water molecule and present results. In Section IVA we derive the multimode Hamiltonian of water. In Section IVB we describe the computer program that is used to describe H₂O, and in Section IVC we present results.

A. Multimode Hamiltonian of Water

Neglecting Coriolis forces and vibrational angular momentum, the molecular Hamiltonian is given by Equation (20). We now derive the detailed form of the kinetic energy $T = \frac{1}{2} \sum_k P_k^2$. Since true vibrations must be restricted to the plane of the molecule, one need consider only displacements $\Delta x_1, \Delta y_1, \Delta x_2, \Delta y_2, \Delta x_3, \text{ and } \Delta y_3$ to describe them. Through the use of symmetry, a combination of the above displacements might be more convenient. In particular, we are looking for combinations that are symmetric or antisymmetric with respect to reflection in the y-z plane of symmetry of the molecule. The combinations must also preserve a fixed center of mass, which requires that

$$\begin{aligned} M_x \Delta x_1 + M_y (\Delta x_2 + \Delta x_3) &= 0 \\ M_x \Delta y_1 + M_y (\Delta y_2 + \Delta y_3) &= 0 \end{aligned} \tag{25}$$

Each of the three vibrations illustrated in Figure 4 can be described by a displacement, S_1 . In Figure 4a, if both M_y masses moved downward a distance S_1 , M_x must move according to Equation (25) to preserve the center-of-mass position:

$$\Delta y_1 = -\frac{M_y}{M_x} (\Delta y_2 + \Delta y_3) = \frac{M_y}{M_x} 2S_1 = 2 \frac{M_y}{M_x} S_1$$

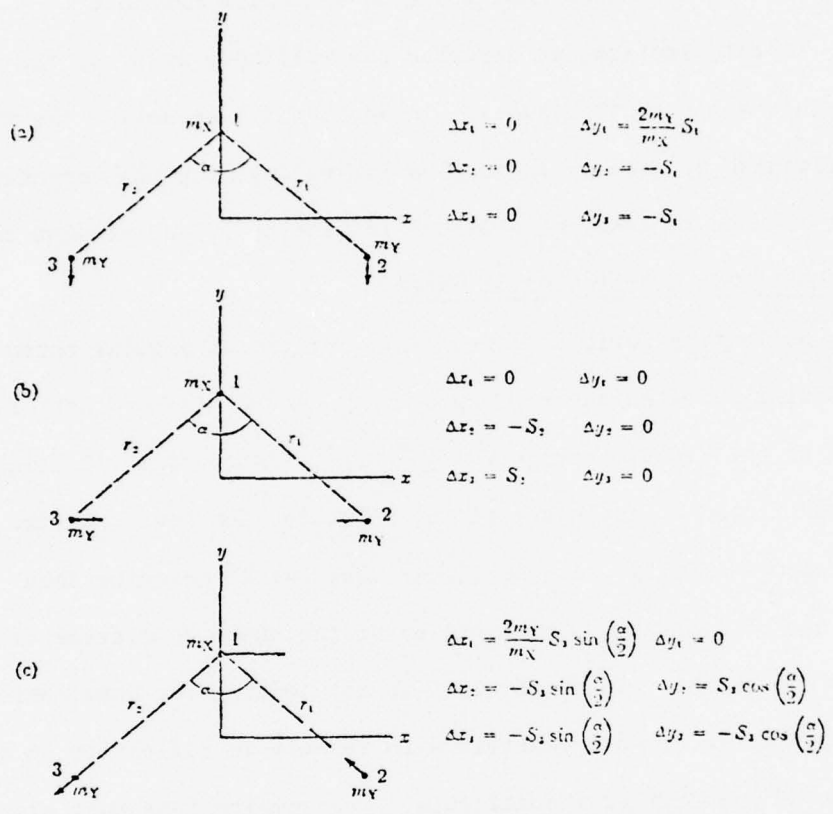


Figure 4. Vibrational displacement coordinates for a nonlinear symmetric molecule.

All $\Delta x_i = 0$ in Figure 4a, and the coordinate S_1 is symmetric with respect to reflection in the y - z plane ("flipping" the molecule over does not disturb the direction of the deflections). In Figure 4b, $\Delta x_2 = -S_2$; $\Delta x_3 = S_2$, and from Equation (23)

$$\Delta x_1 = -\frac{M_y}{M_x} (-S_2 + S_2) = 0$$

all $\Delta y_i = 0$, and S_2 is also a symmetric coordinate. In the third vibration, $\Delta x_{2,3}$ will be some fraction, a , of S_3 ; $\Delta y_{2,3}$ will be a fraction, b , such that

$$\Delta x_2 = -aS_3; \Delta x_3 = aS_3$$

$$\Delta y_2 = bS_3; \Delta y_3 = -bS_3$$

Therefore, Equations (25) yield

$$\Delta x_1 = \frac{2M_y}{M_x} aS_3$$

$$\Delta y_1 = 0$$

Since angular momentum about the z axis must be zero, it can be shown for small vibrations that the M_y 's move along the x - y bonds, and

$$a = \sin \frac{\alpha}{2}; \quad b = \cos \frac{\alpha}{2} \quad (24)$$

S_3 is antisymmetric with respect to reflection. Now any arbitrary vibration of the molecule can be expressed as a linear combination of the symmetry displacements, S_i :

$$\Delta x_1 = \frac{2M_y}{M_x} S_3 \sin \frac{\alpha}{2} \quad \Delta y_1 = \frac{2M_y}{M_x} S_1$$

$$\Delta x_2 = -S_2 - S_3 \sin \frac{\alpha}{2} \quad \Delta y_2 = -S_1 + S_3 \cos \frac{\alpha}{2}$$

$$\Delta x_3 = S_2 - S_3 \sin \frac{\alpha}{2} \quad \Delta y_3 = -S_1 - S_3 \cos \frac{\alpha}{2}$$

and since

$$\dot{x}_1 = \frac{dx_1}{dt} = \frac{d\Delta x_1}{dt} = \frac{2M_y}{M_x} \dot{S}_3 \sin \frac{\alpha}{2}$$

and likewise for \dot{y}_2, \dot{y}_1 etc., the vibrational kinetic energy becomes

$$\begin{aligned} 2T_{\text{vib}} &= M_x(\dot{x}_1^2 + \dot{y}_1^2) + M_y(\dot{x}_2^2 + \dot{y}_2^2 + \dot{x}_3^2 + \dot{y}_3^2) \\ &= 2M_y(\beta \dot{S}_1^2 + \dot{S}_2^2 + \gamma \dot{S}_3^2) \end{aligned} \quad (26)$$

where

$$\beta = 1 + \frac{2M_y}{M_x}; \quad \gamma = 1 + \frac{2M_y}{M_x} \sin^2 \frac{\alpha}{2}.$$

Common practice has been to express the potential energy function of the molecule in terms of bond length stretching and bond angle bending. In Figure 5 δr_1 and δr_2 are the changes in the equilibrium bond length ℓ . $\delta \alpha$ is the change in the angle, α .

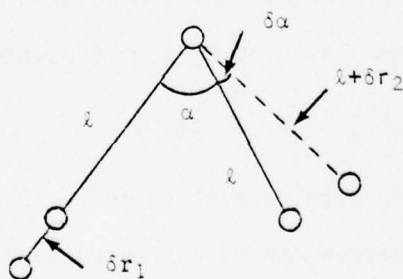


Figure 5. Example of the changes in the equilibrium bond length.

In the limit of small vibrations,

$$\begin{aligned}
 \delta r_1 &= \beta S_1 \cos \frac{\alpha}{2} - S_2 \sin \frac{\alpha}{2} - \gamma S_3 \\
 \delta r_2 &= \beta S_1 \cos \frac{\alpha}{2} - S_2 \sin \frac{\alpha}{2} + \gamma S_3 \\
 \delta \alpha &= \frac{-2\beta S_1 \sin \alpha/2 - 2S_2 \cos \alpha/2}{\ell}
 \end{aligned}
 \tag{27}$$

Let us now define a set of three dimensionless coordinates, in terms of δr_1 , δr_2 , and $\delta \alpha$, which will serve to describe the symmetric stretch, the bending mode, and the asymmetric stretch, respectively:

$$\begin{aligned}
 q_1 &= \frac{\delta r_1 + \delta r_2}{2\ell} = \frac{\beta S_1 \cos \alpha/2 - S_2 \sin \alpha/2}{\ell} \\
 q_2 &= \delta \alpha = \frac{-2\beta S_1 \sin \alpha/2 - 2S_2 \cos \alpha/2}{\ell} \\
 q_3 &= \frac{\delta r_2 - \delta r_1}{2\ell} = \frac{\gamma}{\ell} S_3
 \end{aligned}
 \tag{28}$$

Solve for S_i in terms of the q_i :

$$\begin{aligned}
 S_1 &= \frac{\ell}{\beta} \left(q_1 \cos \frac{\alpha}{2} - \frac{1}{2} q_2 \sin \frac{\alpha}{2} \right) \\
 S_2 &= -\ell \left(q_1 \sin \frac{\alpha}{2} + \frac{1}{2} q_2 \cos \frac{\alpha}{2} \right) \\
 S_3 &= \frac{\ell}{\gamma} q_3.
 \end{aligned}$$

Recalling the kinetic energy, Equation (26), we calculate

$$\begin{aligned}
 \beta \dot{S}_1^2 &= \frac{\ell^2}{\beta} \left(\dot{q}_1^2 \cos^2 \frac{\alpha}{2} - \dot{q}_1 \dot{q}_2 \cos \frac{\alpha}{2} \sin \frac{\alpha}{2} + \frac{1}{4} \dot{q}_2^2 \sin^2 \frac{\alpha}{2} \right) \\
 \dot{S}_2^2 &= \ell^2 \left(\dot{q}_1^2 \sin^2 \frac{\alpha}{2} + \dot{q}_1 \dot{q}_2 \sin \frac{\alpha}{2} \cos \frac{\alpha}{2} + \frac{1}{4} \dot{q}_2^2 \cos^2 \frac{\alpha}{2} \right)
 \end{aligned}$$

and from Equation (26)

$$\begin{aligned}
T &= M_H \ell^2 \left[\left(\frac{\cos^2 \alpha/2}{\beta} + \sin^2 \frac{\alpha}{2} \right) \dot{q}_1^2 \right. \\
&\quad \left. + \frac{1}{2} \sin \alpha \left(1 - \frac{1}{\beta} \right) \dot{q}_1 \dot{q}_2 + \frac{1}{4} \left(\frac{\sin^2 \alpha/2}{\beta} + \cos^2 \frac{\alpha}{2} \right) \dot{q}_2^2 + \frac{\dot{q}_3^2}{\gamma} \right] \\
&= M_H \ell^2 (a_{11} \dot{q}_1^2 + 2a_{12} \dot{q}_1 \dot{q}_2 + a_{22} \dot{q}_2^2 + a_{33} \dot{q}_3^2) \quad (29)
\end{aligned}$$

where

$$\begin{aligned}
a_{11} &= \frac{1}{\beta} \left(\cos^2 \frac{\alpha}{2} + \beta \sin^2 \frac{\alpha}{2} \right) = \frac{1}{\beta} \left(1 + \frac{2M_H}{M_O} \sin^2 \frac{\alpha}{2} \right) = \frac{\gamma}{\beta} \\
a_{12} &= \frac{1}{4} \sin \alpha \left(1 - \frac{1}{\beta} \right) = \left(\frac{M_H}{2M_O} \right) \sin \alpha \\
a_{22} &= \frac{1}{4\beta} \left(\sin^2 \frac{\alpha}{2} + \beta \cos^2 \frac{\alpha}{2} \right) = \frac{1}{4\beta} \left(1 + \frac{2M_H}{M_O} \cos^2 \frac{\alpha}{2} \right) = \frac{\bar{\gamma}}{4\beta} \\
a_{33} &= \frac{1}{\gamma}
\end{aligned}$$

and

$$\begin{aligned}
\gamma &= 1 + \frac{2M_H}{M_O} \sin^2 \frac{\alpha}{2} \\
\bar{\gamma} &= 1 + \frac{2M_H}{M_O} \cos^2 \frac{\alpha}{2} \quad (30)
\end{aligned}$$

Next, calculate the conjugate momenta $P_i = \partial T / \partial \dot{q}_i$:

$$\begin{aligned}
P_1 &= \frac{\partial T}{\partial \dot{q}_1} = 2I_O (a_{11} \dot{q}_1 + a_{12} \dot{q}_2) \\
P_2 &= \frac{\partial T}{\partial \dot{q}_2} = 2I_O (a_{12} \dot{q}_1 + a_{22} \dot{q}_2) \\
P_3 &= \frac{\partial T}{\partial \dot{q}_3} = 2I_O a_{33} \dot{q}_3
\end{aligned}$$

where

$$I_O = M_H \ell^2 \quad (31)$$

and solve for the \dot{q}_i in terms of \dot{P}_i :

$$\dot{q}_1 = \frac{1}{2I_0} \frac{a_{22}P_1 - a_{12}P_2}{a_{11}a_{22} - a_{12}^2}$$

$$\dot{q}_2 = \frac{1}{2I_0} \frac{a_{11}P_2 - a_{12}P_1}{\omega}$$

$$\dot{q}_3 = \frac{1}{2I_0 a_{33}} P_3$$

where

$$\omega \equiv a_{11}a_{22} - a_{12}^2$$

With Equation (28) in mind, form

$$\dot{q}_1^2 = \frac{1}{4I_0^2} \frac{a_{22}^2 P_1^2 - 2a_{12}a_{22}P_1P_2 + a_{12}^2 P_2^2}{\omega^2}$$

$$\dot{q}_2^2 = \frac{1}{4I_0^2} \frac{a_{11}^2 P_2^2 - 2a_{11}a_{12}P_1P_2 + a_{12}^2 P_1^2}{\omega^2}$$

$$\dot{q}_1 \dot{q}_2 = \frac{1}{4I_0^2} \frac{a_{11}a_{22}P_1P_2 - a_{12}a_{22}P_1^2 - a_{11}a_{12}P_2^2 + a_{12}^2 P_1P_2}{\omega^2}$$

Substituting the above into Equation (28), collect the coefficients of the momentum type terms:

$$\begin{aligned} P_1^2: \quad a_{11}a_{22}^2 + a_{22}a_{12}^2 - 2a_{12}^2a_{22} &= a_{11}a_{22}^2 - a_{12}^2a_{22} \\ &= a_{22}\omega \end{aligned}$$

$$\begin{aligned} P_2: \quad a_{11}a_{12}^2 + a_{22}a_{11}^2 - 2a_{11}a_{12}^2 &= a_{22}a_{11}^2 - a_{11}a_{12}^2 \\ &= a_{11}\omega \end{aligned}$$

$$\begin{aligned} P_1P_2: \quad -2a_{11}a_{12}a_{22} - 2a_{11}a_{12}a_{22} + 2a_{11}a_{22}a_{12} + 2a_{12}^3 & \\ &= -2a_{12}\omega \end{aligned}$$

so that

$$T = \frac{1}{4I_0} \left(\frac{a_{22}P_1^2 - 2a_{12}P_1P_2 + a_{11}P_2^2}{\omega} + \frac{P_3^2}{a_{33}} \right)$$

Simplifying ω ,

$$\begin{aligned}
 \omega &= \frac{\gamma}{\beta} \frac{\bar{\gamma}}{4\beta} - \left(\frac{M_H}{2M_0\beta} \right)^2 \sin^2\alpha \\
 &= \frac{1}{4\beta^2} (\gamma\bar{\gamma} - \chi^2 \sin^2\alpha) \\
 &= \frac{1}{4\beta^2} \left[\left(1 + 2\chi \sin^2 \frac{\alpha}{2} \right) \left(1 + 2\chi \cos^2 \frac{\alpha}{2} \right) - \chi^2 \sin^2\alpha \right] \\
 &= \frac{1}{4\beta^2} \left(1 + 2\chi + 4\chi^2 \sin^2 \frac{\alpha}{2} \cos^2 \frac{\alpha}{2} - \chi^2 \sin^2\alpha \right) \\
 &= \frac{1}{4\beta^2} (1 + 2\chi) = \frac{1}{4\beta}
 \end{aligned}$$

therefore

$$T = \frac{\beta}{I_0} \left(a_{22}P_1^2 - 2a_{12}P_1P_2 + a_{11}P_2^2 \right) + \frac{P_3^2}{4I_0a_{22}} \quad (32)$$

This is the final form of the kinetic energy for a multimode calculation where the a_{ij} are given in Equation (50). Notice that if either mode one or two is considered separately, so that no interaction exists, $a_{12} = 0$, and

$$\omega \equiv a_{11}a_{22} - a_{12}^2 = a_{11}a_{22}$$

Therefore,

$$\begin{aligned}
 T &= \frac{1}{4I_0} \left(\frac{a_{22}P_1^2 - 2a_{12}P_1P_2 + a_{11}P_2^2}{\omega} + \frac{P_3^2}{a_{33}} \right) \\
 &= \frac{1}{4I_0} \left(\frac{P_1^2}{a_{11}} + \frac{P_2^2}{a_{22}} + \frac{P_3^2}{a_{33}} \right) \quad (33)
 \end{aligned}$$

1. Rotation Constants

The inverse moments of inertia (rotation constants) are calculated as follows:

$$\begin{aligned}
 I_{yy} &= \sum_i M_i x_i^2 = 2M_H C^2 = 2M_H \left(r \sin \frac{\theta}{2} \right)^2 \\
 &= 2M_H r^2 \sin^2 \frac{\theta}{2} = M_H r^2 (1 - \cos \theta)
 \end{aligned} \tag{34}$$

$$\begin{aligned}
 I_{xx} &= \sum_i M_i y_i^2 = 2M_H b^2 + M_O (a - b)^2 \\
 &= \frac{M_H M_O}{M_{mol}} r^2 (1 + \cos \theta)
 \end{aligned} \tag{35}$$

$$I_{zz} = I_{xx} + I_{yy} \tag{36}$$

where

$$M_{mol} = 2M_H + M_O$$

If $q_2 \equiv 2 \sin(\theta/2)$ (the alternate description of the bending mode), then

$$I_{xx} = \frac{M_H M_O}{M_{mol}} r^2 (2 - q_2^2 \alpha / 2) \tag{37}$$

$$I_{yy} = M_H r^2 (q_2^2 \alpha / 2)$$

In both Equations (34) and (35) above, the value r may vary, if the symmetric or asymmetric stretch is being considered. Defining the average r^2 as the average of the squares of the separate bond lengths,

$$\begin{aligned}
 r^2 &= \frac{r_1^2 + r_2^2}{2} \\
 &= \frac{2(\bar{r}^2 + \bar{r} \Delta r_1 + \bar{r} \Delta r_2) + \Delta r_1^2 + \Delta r_2^2}{2}
 \end{aligned} \tag{38}$$

where

$$r_1 = \bar{r} + \Delta r_1$$

$$r_2 = \bar{r} + \Delta r_2$$

Therefore, Equation (38) yields

$$r^2 = [\lambda^2 + \lambda^2(q_1 - q_3) + \lambda^2(q_1 + q_3)] + \frac{\lambda^2}{2} (q_1^2 + 2q_1q_3 + q_3^2) + \frac{\lambda^2}{2} (q_1^2 - 2q_1q_3 + q_3^2) = \lambda^2(1 + 2q_1 + q_1^2 + q_3^2)$$

In any calculation involving either mode one or mode three, the moment of inertia may be factored into bending and stretching integrals:

$$\langle ik | I_{yy} | j \ell \rangle = \langle i | R(q_{1,3}) | j \rangle * \langle k | (1 - \cos\theta) | \ell \rangle$$

where

$$R(q_1) = M_H \lambda^2 (1 + 2q_1 + q_1^2)$$

$$R(q_3) = M_H \lambda^2 (1 + q_3^2)$$

Thus a two-mode calculation with either stretch requires two one-dimensional integrals. A three-mode calculation would require a two-dimensional integral over $R(q_1, q_3)$. Finally,

$$A_{ij} = \langle i | \frac{1}{I_{xx}} | j \rangle \quad (39)$$

$$B_{ij} = \langle i | \frac{1}{I_{yy}} | j \rangle \quad (40)$$

$$C_{ij} = \langle i | \frac{1}{I_{zz}} | j \rangle \quad (41)$$

B. Description of Computer Code

The multivibrational mode molecular physics program known as MISERE is currently capable of producing full three-mode vibrational wave functions for H₂O and similar nonlinear symmetric triatomic molecules. The rotation constants, from which is calculated the rotational energy spectrum, are presently restricted to two-mode analyses, mainly for convenience. While several of the routines comprising this program are general and may be applied to much more complex systems, others are entirely problem dependent. The modularization of the code, however, enables a versatility that makes treatment of more complex models a relatively easy task.

In the discussion that follows, the three main products of the calculation (vibrational eigenfunctions, rotation constants and rotational energies) will be broken down in terms of the individual routines that produce them.

1. Vibrational Wave Functions

The main routine first calls SETUPM, which almost entirely defines the current problem. It sets up the molecular geometry (masses, angles, and bond lengths), chooses a coordinate system, and defines the kinetic energy operators in terms of the chosen coordinates. MAIN then calls WAVEFN, which will produce the eigenfunctions for the molecule just set up. WAVEFN first needs the integrals that will comprise the Hamiltonian matrix, so it calls INTGRT to calculate (1) the kinetic integrals (P² type terms); (2) the P type terms that will participate in kinetic interactions between modes; (3) the potential matrix elements

(choice of power series or Morse potentials); and (4) the matrix of various coordinate moments ($\langle i|q^n|j\rangle$) that will describe the interactions of the potentials between modes. These integrals are calculated and stored for each normal mode. INTGRT will presently produce up to 10 basis functions (Harmonic or Morse) per mode, but is practically limited only by storage and some minor adjustments. Harmonic oscillator matrix elements are analytically derived using raising and lowering operators. Morse eigenenergies are also analytically calculated, but P type terms and coordinate moments are integrated using a Gauss-Hermite 12-point numerical integration. INTGRT is virtually problem independent.

Having at hand the integrals needed for the Hamiltonian and the parameters controlling the sizes of the potential terms and interactions (from input or fitting procedure), one needs only to assemble the various terms into a coherent Hamiltonian. This is the job of ORGANZ. ORGANZ takes the matrix of integrals produced by INTGRT and stores them wherever required in the multimode Hamiltonian. This routine is also problem independent, and theoretically will handle any number of modes. We discuss here only fundamental limitations.

All that remains of the vibrational calculation is to diagonalize the Hamiltonian. We use a variable threshold Jacobi method, JACVAT, which gives reasonably fast and accurate eigenvalues and vectors for medium size matrices. The vibrational energy spectrum that has now been produced may be compared to experiment and, if desired, an iteration may be set up to fit the calculated energy spacings to experimental values. If so instructed, WAVEFN will call a nonlinear function minimi-

zation routine, STEPIT, which will fit the energy spacings to measured values by simultaneously varying the potential parameters. STEPIT is a standard routine using a direct search method (no derivatives) with automatic step size adjustment and acceleration. Also adjusted during the fit procedure is the frequency of the ground state vibration. By minimizing the ground state Hamiltonian, one in effect optimizes the choice of basis set.

2. Rotation Constants

If desired, MAIN will next call ROTMAT, which calculates single or double mode rotation constants (the bending mode alone, or in conjunction with either stretch mode). The convenience of the present setup is due to the fact that the double mode calculation can be factored into two one-dimensional integrations. A three-mode analysis would require a two-dimensional integral over the stretch coordinates. ROTMAT first calls INTROT, a separate entry point in INTGRT, to get the inverse inertia moment integrals. The integrals defined in INTGRT are problem dependent (on geometry and coordinate system), but otherwise the 12-point Gauss-Hermite integrations are general. Morse or Harmonic basis sets are available. ROTMAT then assembles the integrals into rotation matrices, reduces the matrix to contain bands of interest to subsequent calculations, and similarity transforms the reduced matrix to the eigenvector basis found in WAVEFN.

At this point, MAIN will optionally adjust the molecular geometry to fit selected rotation constants. At present, STEPIT varies the bond angle and equilibrium O-H bond length to fit exactly the experimental ground state A and B rotation constants.

3. Rotational Energies

If rotation constants have been calculated, MAIN will optionally use them to derive the rotational energy spectrum for the vibrational bands specified in the previous step. ROTENG will call WANG, which forms the vibrational-rotational Hamiltonian. WANG utilizes the WANG transformation, which factors the Hamiltonian into four smaller matrices that can be diagonalized separately by JACVAT. This saves much time and space, but restricts the analysis to asymmetric rotor type molecules.

C. Molecular Potential Surface and Geometry

It was decided that the following form of the potential will produce wavefunctions that will best reproduce the rotational-vibrational spectrum of H₂O:

$$V(q_1, q_2) = D_1[1 - \exp(-\beta_1 q_1)]^2 + D_2[1 - \exp(-\beta_2 q_2)]^2 \\ + D_{12} q_1 [1 - \exp(-\beta_2 q_2)]^2 + D_{21} q_2 [1 - \exp(-\beta_1 q_1)]^2$$

This potential involves six free parameters that were least-squares fit to four fundamental (100,200,010,020) and two combination (110,120) vibrational bands. In addition, the geometric parameters of the molecule r_0 and θ_0 were varied self-consistently during the vibrational fit, so that the ground state A and B constants matched the experiment. The static geometry of the molecule is

$$r_0 = 0.9862 \text{ \AA} \quad \theta_0 = 104.33^\circ$$

The vibrational spacings were considered fit when within 1 cm⁻¹ of experiment. The final values of the potential parameters are (in cm⁻¹):

$$\begin{array}{lll} D_1 = 65284 & q_1 = 2.46 & D_{12} = -24559 \\ D_2 = 36073 & q_2 = 0.7095 & D_{21} = -5326 \end{array}$$

A stability analysis was performed to see the effect of expanding the original basis set of three Morse functions per mode. It was apparent that no significant difference occurred that would warrant a larger set, and indeed, the predicted 030 vibrational spacing was within 0.06% of experiment.

Table 22 shows 101 rotational energies, calculated from rotation constants predicted by the above potential.

Table 22

Rotational Energies Calculated from Rotation Constants

Band	J	τ	Calculated (cm^{-1})	Observed (cm^{-1})	Dev. (%)
090	1	-1	23.709	23.890	0.04
090	1	0	37.091	37.140	0.16
090	1	1	42.337	42.370	0.08
100	1	-1	3680.056	3680.453	0.01
100	1	0	3692.819	3693.293	0.01
100	1	1	3698.052	3698.489	0.01
010	1	-1	1618.383	1618.000	0.02
010	1	0	1634.757	1633.000	0.01
010	1	1	1640.317	1640.000	0.02
110	1	-1	5259.955	5258.000	0.04
110	1	0	5275.193	5274.000	0.02
110	1	1	5282.718	5280.000	0.05
020	1	-1	3175.232	3175.000	0.01
020	1	0	3196.137	3196.000	0.00
020	1	1	3201.922	3202.069	0.00
090	2	-2	70.069	70.090	0.12
090	2	-1	79.470	79.493	0.03
090	2	0	95.166	95.175	0.01
100	2	-2	3735.498	3735.943	0.01
100	2	-1	3734.437	3734.894	0.01
100	2	0	3750.123	3750.466	0.01
100	2	1	3787.753	3788.694	0.02
100	2	2	3789.064	3789.974	0.02
010	2	-2	1664.670	1665.000	0.02
010	2	-1	1676.910	1677.000	0.01
010	2	0	1693.463	1693.620	0.01
010	2	1	1741.444	1743.000	0.09
010	2	2	1742.623	1743.640	0.06
110	2	-2	5397.898	5394.000	0.07
110	2	-1	5317.531	5315.000	0.05
110	2	0	5340.131	5332.000	0.15
110	2	1	5325.627	5379.000	0.14
110	2	2	5333.734	5320.000	0.16
020	2	-2	3222.042	3222.000	0.00
020	2	-1	3237.809	3233.000	0.01
020	2	0	3255.350	3255.000	0.01
020	2	1	3320.026	3316.000	0.12
020	2	2	3321.057	3317.000	0.12
090	3	-3	136.594	136.755	0.18
100	3	-3	3790.839	3791.375	0.01
100	3	0	3858.431	3858.279	0.01
100	3	3	3932.644	3935.346	0.07
010	3	-3	1731.325	1732.000	0.04
010	3	0	1813.433	1814.000	0.03
110	3	-3	5375.195	5370.000	0.10
020	3	-3	3290.039	3289.000	0.03
020	3	0	3399.467	3383.000	0.07
100	4	-4	3874.627	3875.017	0.02
100	4	0	3966.697	3966.555	0.00
010	4	-4	1816.552	1817.000	0.02
010	4	0	1921.845	1923.000	0.06
110	4	-4	5459.764	5454.000	0.11
020	4	-4	3377.240	3375.000	0.07
020	4	0	3499.745	3496.000	0.11
100	5	-5	3975.895	3976.304	0.01
100	5	0	4150.305	4150.288	0.00
010	5	-5	1919.576	1921.000	0.07
010	5	0	2124.911	2127.000	0.10
110	5	-5	5561.121	5555.000	0.11
020	5	-5	3482.079	3479.000	0.09

BEST AVAILABLE COPY

BEST AVAILABLE COPY

Table 22. Continued

Band	J	τ	Calculated (cm^{-1})	Observed (cm^{-1})	Dev. (%)
000	6	-6	445.815	446.695	0.20
100	6	-6	4095.078	4095.313	0.01
100	6	0	4305.289	4308.213	0.05
010	6	-6	2040.329	2042.000	0.03
010	6	0	2278.445	2283.000	0.20
110	6	-6	5679.635	5673.000	0.12
020	6	-6	3604.252	3609.000	0.12
000	7	-7	585.130	586.000	0.15
100	7	-7	4231.873	4232.000	0.00
100	7	-5	4347.723	4348.000	0.01
100	7	-3	4423.526	4426.000	0.06
100	7	-1	4481.166	4485.000	0.09
100	7	1	4569.949	4572.000	0.05
100	7	3	4639.698	4696.000	0.15
010	7	-7	2173.925	2181.000	0.10
110	7	-7	5315.620	5310.000	0.10
020	7	-7	3744.367	3739.000	0.14
000	8	-8	742.688	744.000	0.18
100	8	-8	4387.970	4387.000	0.02
100	8	-6	4523.739	4524.000	0.01
100	8	-4	4619.487	4623.000	0.03
100	8	-2	4636.677	4689.000	0.05
100	8	0	4766.093	4769.000	0.02
100	8	2	4886.663	4889.000	0.05
010	8	-8	2335.450	2338.000	0.11
110	8	-8	5969.251	5963.000	0.10
020	8	-8	3902.441	3895.000	0.19
000	9	-9	913.502	920.000	0.16
100	9	-9	4561.056	4560.000	0.02
100	9	-7	4717.477	4716.000	0.03
100	9	-5	4834.264	4833.000	0.02
100	9	-3	4913.040	4913.000	0.19
100	9	-1	4991.773	4996.000	0.03
100	9	1	5108.040	5108.000	0.00
010	9	-9	2509.977	2513.000	0.12
110	9	-9	6140.629	6135.000	0.09
100	10	-10	4734.159	4739.373	0.03
100	10	-8	4929.237	4935.897	0.07
100	10	-6	5046.612	5069.000	0.04
100	10	-4	5161.534	5169.033	0.15
100	10	-2	5240.893	5246.892	0.11

REFERENCES

1. N. Darling and B. Dennison, *J. Chem. Phys.* 3, 102 (1938).
2. C. Townes and M. Schawlow, *Microwave Spectroscopy* (Addison-Wesley, New York, 1961).
3. J. K. G. Watson, *J. Chem. Phys.* 45, 1360 (1966).
4. J. K. G. Watson, *Molecular Phys.* 15, 479 (1968).
5. M. Born and J. R. Oppenheimer, *Ann. Physik* 84, 457 (1927).
6. F. DeLucia, P. Helminger, R. Cook, and W. Gordy, *Phys. Rev.* 85, 487 (1976).
7. L. Pugh and K. Rao, *J. Molecular Spectroscopy* 47, 403 (1973).
8. The energy of the (020) state lies at 3150 wavenumbers above the ground state.
9. R. T. Hall and J. N. Dowling, *J. Chem. Phys.* 47, 2454 (1967).
10. D. Rogovin and H. Tigelaar, contract report on "Spectroscopic Modeling of the Water Molecule," prepared for AFWL, Kirtland Air Force Base, New Mexico, November 1974.
11. W. S. Bendick, H. S. Classen, and J. H. Shore, *J. Res. National Bureau Standards* 49, 91 (1954).